Faculty of Physics and Astronomy

University of Heidelberg

Diploma thesis
in Physics

submitted by

Marc Deissenroth

born in Salzkotten

May 2005

Optimization and Realization of a Neutrino Asymmetry Measurement in the Decay of Polarized Neutrons

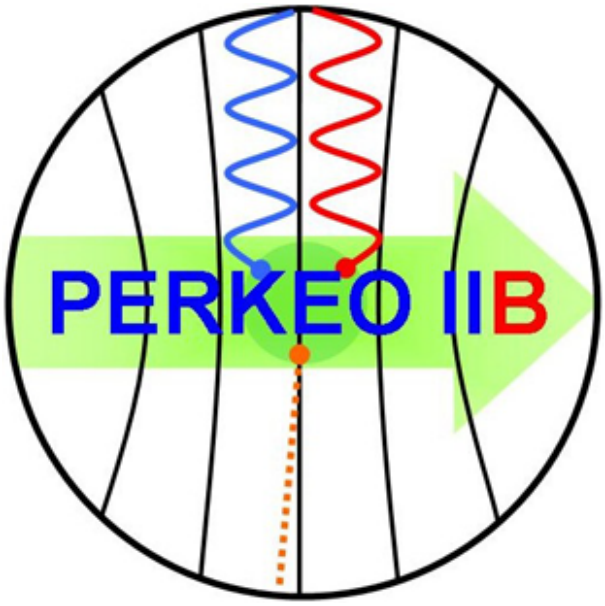

This diploma thesis has been carried out by
Marc Deissenroth
at the Physics Institute of the University of Heidelberg
under the supervision of
Priv.-Doz. Dr. Hartmut Abele.

May 2005

Abstract

Optimization and Realization of a Neutrino Asymmetry Measurement in the Decay of Polarized Neutrons

We report on the precision measurement of the neutrino asymmetry B. This correlation between neutron spin and momentum of the neutrino is obtained in the β-decay of free polarized neutrons using the spectrometer PERKEO II. Compared to the last B-measurement we improved the setup at several points: We used two supermirror polarizers in a crossed geometry and obtained a polarization efficiency of 99.7(1) %. In addition, a new data acquisition system allowed to reduce systematic effects.

Furthermore, we developed a Monte Carlo Simulation software for a better understanding of systematic effects and background. Corrections on asymmetry B spectra due to the magnetic mirror effect are obtained and we can show that the considered corrections are small and less than 0.04 % in the region of interest.

Zusammenfassung

Optimierung und Durchführung einer Neutrino-Asymmetrie Messung im Zerfall polarisierter Neutronen

Wir berichten über die Präzisionsmessung der Neutrino Asymmetry B. Diese Korrelation zwischen dem Neutronenspin und dem Impuls der Neutrinos, soll im β Zerfall freier, polarisierter Neutronen mit dem Spektrometer PERKEO II bestimmt werden. Im Vergleich zur letzten B Messung wurde das Experiment an mehreren Stellen verbessert: Durch die Verwendung zweier gekreuzter Polarisatoren erhielten wir eine Polarisationseffizienz von 99.7(1) %. Zudem verwendeten wir ein neues System zur Datenaufnahme, wodurch systematisches Effekte verringert wurden.

Weiterhin wurde eine Monte Carlo Simulation programmiert, um systematische Effekte und den Untergrund besser verstehen zu können. Wir erhalten Korrekturen auf die Asymmetrie B Spektren aufgrund des magnetischen Spiegeleffekts. Diese Korrekturen sind kleiner als 0.04 % im relevanten Energiebereich.

This thesis is dedicated to my parents and to everyone who has supported me on my way through the world of physics.

Contents

Chapter 1

Introduction

The Standard Model of particle physics includes the theories of electromagnetic, weak and strong interactions. Every experiment that verifies predictions made by the Standard Model confirms this very succesful theory. But there are also many open questions : Why, for example, is parity maximally violated. Hence physicists are searching for "Physics beyond the Standard Model".
Alternative models try to explain the present world with theories that are also valid at the beginning of the universe. Many of these theories claim, that the early universe was right-left symmetric, and parity violation arises due to spontaneous symmetry breaking. Then small amounts of right handed currents would still be present today, and parity would not be violated maximally.

PERKEO II is a high precision experiment to examine neutron decay: It checks predictions of the Standard Model and searches for "new physics". The topic of this thesis is the measurement of the neutrino asymmetry B with PERKEO II[1]: This coefficient describes the correlation between neutron spin and neutrino momentum. It is therefore very sensitive to admixtures of right handed currents, and a precise determination of the asymmetry B gives constraints on theories beyond the Standard Model. Therefore we made much effort to increase the precision of the measurement: The setup of the experiment was improved to reduce corrections and uncertainties, and simulations were made for a better understanding of systematic effects.

Chapter 1 gives a short introduction to the theory and introduces PERKEO II. The experiment itself is described in Chapter 2. Here we present the improvements of the setup compared to the experiment done in 2001 [Kre04] [Kre05a], and describe the alignment of the neutron beam to the magnetic field. The Monte Carlo Simulation software (Chapter 3) was developed for a better understanding of systematic effects and background. We simulate the influence of the magnetic mirror effect and the edge effect on the spectra and give corrections on the measured spectra. The last chapter presents an outlook on the new spectrometer PERKEO III, designed to determine the correlation coefficients with highest accuracy.

[1] During the same measuring campaign with the same apparatus, also electron asymmetry A and proton asymmetry C has been measured

Chapter 2

PERKEO Overview

In this chapter we will give a brief overview on phenomenology and theory of the neutron decay and weak interactions as given in the Standard Model of particle physics. We introduce the correlation coefficients (asymmetries) occurring in neutron decay and show possible deviations due to "Physics beyond the Standard Model". In the second part we describe PERKEO II, the experiment we used to measure the neutrino asymmetry B.

2.1 Theory

2.1.1 The Neutron and the Neutron Decay

The Beginning: Among the particles of the Standard Model, the neutron discovered by *Chadwick* in 1932 certainly belongs to one of the most studied and best known baryons. The neutron is a spin-$\frac{1}{2}$ particle consisting of the three valence quarks (u,d,d). Its mass in natural units ($\hbar = c = 1$) is $m_n = 939.57$ MeV [PDG04] and a free neutron decays with a mean lifetime of $\tau_n = 885.7(8)$ s [PDG04]into a proton, an electron and an antineutrino

$$n \longrightarrow p + e^- + \overline{\nu}_e. \tag{2.1}$$

The expected spectrum of the electron energy is given by the density of states ρ (see e.g [Pov01])

$$d\rho(E_0, E_e) = \frac{V^2}{4\pi^4} E_e \sqrt{E_e^2 - m_e^2} \cdot (E_0 - E_e)^2 dE_e \tag{2.2}$$

with the phase space factor

$$f(E_0) = E_e \sqrt{E_e^2 - m_e^2} \cdot (E_0 - E_e)^2, \tag{2.3}$$

where V denotes a normalizing volume. E_0 represents the total kinetic energy, that means the sum of the electron kinetic energy E_e and the neutrino energy $E_{\overline{\nu}}$ ($\overline{\nu}$ is assumed to be

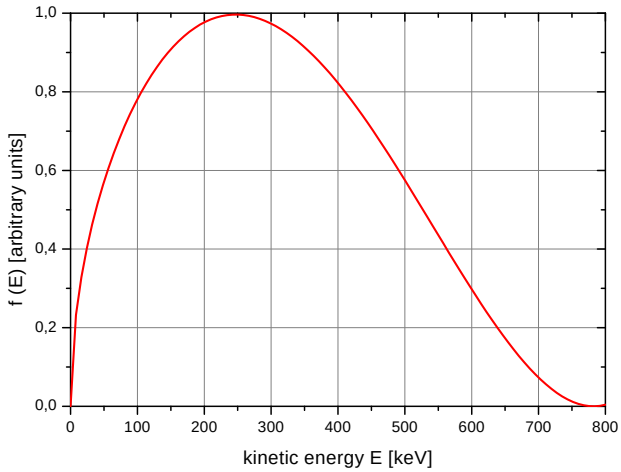

Figure 2.1: The uncorrected phase space factor $f(E_0)$ of the β-spectrum.

massless). Neglecting the proton recoil the endpoint energy is $E_{e,max} = 782$ keV [Pov01]. The spectrum $f(E_0)$ is called *Fermi spectrum* and is shown in figure 2.1.

To obtain a realistic spectrum several theoretic corrections have to be taken into account: The outer radiative correction $\delta_R(E)$, the proton recoil $R_0(E)$ and the Fermi correction $F_C(E)$ to account for the attractive Coulomb force between proton and electron [Bae96]. The Fermi spectrum $f(E_0)$ now reads

$$F(E_0) = f(E_0) \cdot (1 + \delta_R(E))(1 + R_0(E))F_C(E) \tag{2.4}$$

2.1.2 Neutrino Helicity, Electroweak Unification and Quark-Mixing

The hadronic vertex $n \longrightarrow p + W$ can be described on the quark level as a $d \rightarrow u$ transition which is shown in the Feynman graph figure 2.2. The probability for this quark transition is described in V_{ud}, a quantity occuring in weak interactions (see below). V_{ud} may be obtained in neutron β-decay by measuring the electron asymmetry A, a coefficient also measured with PERKEO II [Mun05]. Furthermore, the measured coefficient B is sensitive to the neutrino's helicity, and may give constraints on left-right symmetric models. Therefore, we describe the phenomenology of weak interactions and introduce quark-mixing.

Weak interaction: *Fermi* gave the first theoretical explanation for neutron β-decay. He postulated an effective four-fermion point interaction, in analogy to the electromagnetic interaction mediated by photons. The total matrix element is made up of the *hadronic* and the *leptonic weak current* (both vector currents) matrix elements [Ait89]

$$\mathcal{M} = \langle p|j_\mu|n\rangle\langle e\overline{\nu}_e|j^\mu|0\rangle \tag{2.5}$$

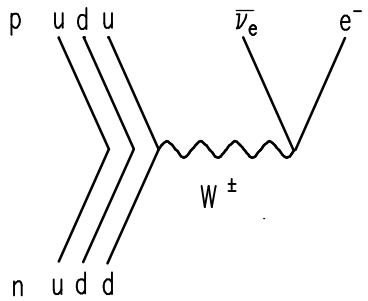

Figure 2.2: Feynman diagram of neutron β-decay.

where j_μ is the four-vector of the transition current, n and p are the quantum mechanical states of the neutron and the proton. Due to the very low energy release, one might ignore all momentum dependencies in the matrix element and can reduce $\mathcal{M}$ in good approximation to a constant, the so called coupling constant G_F. Although *Fermi* followed electromagnetic interactions, there were two important differences that made his theory imperfect: On the one hand, it is hard to see why the $e\overline{\nu}_e$ pair, which varies its effective mass from process to process, should be comparable to the γ-quantum emitted in a radiative transition. On the other hand, the electromagnetic coupling constant α is dimensionless, other than G_F (which has the dimesion Energy^{-2}). To avoid these differences, theoreticians assumed that the weak interaction is mediated by new bosons, namely the $W^\pm$ bosons as mediators of the charged weak current and the Z^0 boson to describe neutral currents.

The new matrix element is given by

$$\mathcal{M} \propto g^2 \cdot \frac{-g^{\mu\nu} + \frac{q^\mu q^\nu}{M_W^2}}{q^2 - M_W^2}, \tag{2.6}$$

with the momentum tranfer $q_\mu = (p_\mu - p'_\mu)$ and $M_W \approx 80$ GeV for the W-boson mass. g is the characteristic coupling strength of weak interactions; it is introduced analog to the coupling constant e in electromagnetic interations. Since there is a very small momentum transfer in neutron decay, $q^2 \ll M_W^2$, one can disregard all terms including q. This results in a constant propagator term which is related to the Fermi constant G_F given above via

$$\frac{G_F}{\sqrt{2}} = \frac{g^2}{8M_W^2}. \tag{2.7}$$

The Fermi constant G_F can be determined precisely in muon decay experiments to a value of $G_F = 1.166 \cdot 10^{-5}$ GeV^{-2} [PDG04].

V-A Theory: Many ingenious experiments confirmed parity violation and evidenced that the neutrino's helicity is always negative or left-handed and antineutrinos are always right-handed. The measured neutrino asymmetry B is associated to the neutrino's helicity,therefore we give a short mathematical description of this effect: One introduces two

projection operators P_R and P_L (the index stands for the projection on right- or left-handed particles) which affect a Dirac spinor u in the way

$$u = \underbrace{(\frac{1+\gamma_5}{2})}_{P_R} u + \underbrace{(\frac{1-\gamma_5}{2})}_{P_L} u \equiv u_R + u_L. \tag{2.8}$$

These operators yield the existence of a vector and an axial-vector current in weak interactions[1] with coefficients c_V and c_A. Parity is maximally violated for $|c_V| = |c_A|$. In fact $c_V = -c_A = 1$, hence the theory is called V-A-theory.

We have also to account for the composite structure of the neutron. In β-decay experiments one can measure the absolute value of the strength of the vector and axial coupling, termed g_V and accordingly g_A. Since one finds $g_V = 1$, strong interactions do not seem to affect vector coupling, what is called the "Conserved Vector Current" (CVC) hypothesis. On the other hand the axial current is affected since one measures $g_A = 1.27$ ("Partially Conserved Axial Current" (PCAC) hypothesis). Adding the factors g_A and g_V in the $n \longrightarrow p + W$ vertex factor we get

$$\mathcal{M} \sim \frac{G_F}{\sqrt{2}} \left(\overline{u}(p)\gamma^\mu (1 + \frac{g_A}{g_V}\gamma^5) u(n) \right) \left(\overline{u}(e)\gamma_\mu (1-\gamma^5) u(\nu_e) \right), \tag{2.9}$$

where u represents the particle spinor and $\overline{u}$ the adjoint spinor: $\overline{u} = u^\dagger \gamma^0$.

One has to distinguish between the following two transitions mediated by vector or axial currents: *Fermi transitions* or vector transitions conserve the nucleon spin in β-decay and the emission of the decay products is isotropic. Observing this transition, no asymmetry will be noticeable and parity will be conserved (see figure 2.3).
Gamow-Teller transitions or axial transitions can cause a spinflip of the hadron. This case violates parity since there is a favoured electron emission direction due to momentum conservation.

Electroweak Unification and Quark Mixing: Since only left-handed fermions (right-handed antifermions) couple to the W-boson, the theory of electroweak unification introduces SU(2)-doublets for left-handed leptons and the Cabibbo-rotated left-handed quarks:

$$\begin{aligned} \text{Leptons} \quad &: \begin{pmatrix} \nu_e \\ e \end{pmatrix}_L, \qquad \begin{pmatrix} \nu_\mu \\ \mu \end{pmatrix}_L, \qquad \begin{pmatrix} \nu_\tau \\ \tau \end{pmatrix}_L \\ \text{Quarks} \quad &: \begin{pmatrix} u \\ d' \end{pmatrix}_L, \qquad \begin{pmatrix} c \\ s' \end{pmatrix}_L, \qquad \begin{pmatrix} t \\ b' \end{pmatrix}_L. \end{aligned}$$

A Cabibbo-rotated quark d' is a superposition of the mass eigenstates d, s and b.

$$d' = V_{ud}\ d + V_{us}\ s + V_{ub}\ b. \tag{2.10}$$

[1] γ^μ alone yields a vector current, whereas $\gamma^\mu\gamma^5$ gives an axial vector, see (2.9).

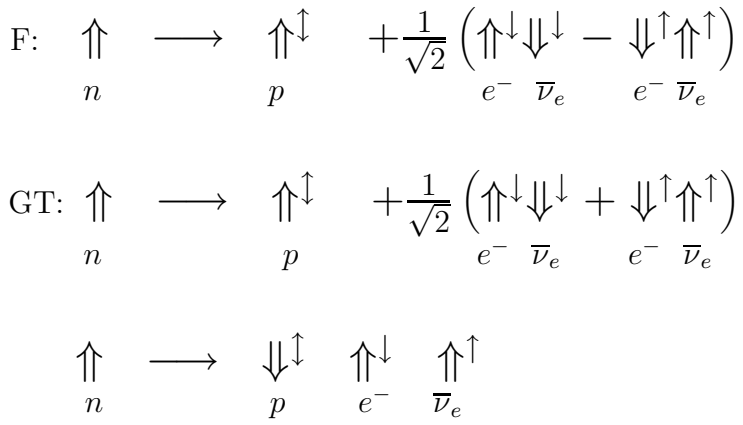

Figure 2.3: The Fermi (F) and Gamow-Teller (GT) transitions in neutron decay. The spin of the particle is indicated by the double arrow, the smaller arrow shows the prefered direction of emission. The second GT transition yields to an anisotropy in the decay. (Figure based on [Rei99].)

This rotated quark is required to keep the coupling of the weak interaction g constant since if the eigenstate d would turn to u the coupling g would decrease by about 4%. The Cabbibo rotation therefore implies universality of the coupling constant g. In general the unitary[2] 3×3 *Cabibbo-Kobayashi-Maskawa matrix* (CKM matrix) describes the mixing of the quark mass eigenstates:

$$\begin{pmatrix} d' \\ s' \\ b' \end{pmatrix} = \begin{pmatrix} V_{ud} & V_{us} & V_{ub} \\ V_{cd} & V_{cs} & V_{cb} \\ V_{td} & V_{ts} & V_{tb} \end{pmatrix} \begin{pmatrix} d \\ s \\ b \end{pmatrix}. \tag{2.11}$$

$|V_{qq'}|^2$ gives the probability that quark q' changes into quark q. The unitarity of the matrix implies for the elements of a row

$$\sum_j |V_{ij}|^2 = 1, \quad i = u, c, t \quad \text{and} \quad j = d, s, b. \tag{2.12}$$

We can therefore check the unitarity condition by determining these matrix elements.

There are different ways to determine the individual matrix elements. The element V_{ud} for example can be obtained from the β-decay of neutrons. Combining this with experimental results for V_{us} and V_{ub}[3] one can confirm or reject the theory [Abe02].

[2]Unitarity means $V^\dagger V = 1$ where $V^\dagger$ is the transposed conjugate of V, i.e. $V^\dagger =^T V^*$.

[3]V_{us} is measured in semileptonic K-decays, B-meson decays give V_{ub}.

The β-decay Matrix Element and Lagrangian: Due to quark mixing, the matrix element (2.9) for the decay is changed to

$$\mathcal{M} = -\frac{G_F}{\sqrt{2}}\, V_{ud}\, \overline{u}(p)\gamma_\mu \left(1 + \frac{g_A}{g_V}\gamma_5\right) u(n)\; \overline{u}(e)\gamma^\mu\,(1-\gamma_5)\, u(\nu_e). \tag{2.13}$$

This matrix element does not yet account for the momentum transfer q_μ from the hadron to the leptons. If we implement currents occuring naturally in the quark model to describe q_μ, the Lagrangian for the neutron decay reads [Abe00]

$$\mathcal{L} = \frac{1}{2}\frac{G_F}{\sqrt{2}}\, \overline{u}(p) \left(\gamma_\mu(1+\lambda\gamma_5) + \frac{g_{wm}}{2m_p}\sigma_{\mu\nu}q^\nu\right) u(n)\; \overline{u}(e)(1-\gamma_5)u(\nu). \tag{2.14}$$

$g_{wm} = \mu_p - \mu_n$ is the difference between the magnetic moment of the proton and the neutron, the so called weak magnetism. $\lambda = \frac{g_A}{g_V}$ is the ratio of the coupling constants and m_p indicates the proton mass.

2.1.3 Observables in Neutron Decay

The decay probability $w(E)$ for a neutron is given by Fermi's Golden Rule

$$w(E)dE = 2\pi|\mathcal{M}|^2 \cdot d\rho(E_0, E), \tag{2.15}$$

where $d\rho(E_0, E)$ is given in (2.2) and the matrix element for unpolarized neutrons is

$$|\mathcal{M}|^2 = g_V^2 + 3g_A^2. \tag{2.16}$$

Combining (2.2), (2.15), and (2.16) we get

$$w(E)dE \propto G_F^2\; V_{ud}^2\; f(E_0)\; (g_V^2 + 3g_A^2). \tag{2.17}$$

The observables of the experiment are the energies of the decay products and their relative emission directions. *Jackson* gave a parametrization for the transition probability in case of polarized neutrons [Jac57]:

$$\begin{aligned} \mathrm{d}\omega \;&\propto\; G_F^2\,|V_{ud}|^2\; f(E_0)\; (g_V^2 + 3g_A^2)\; \mathrm{d}E\; \mathrm{d}\Omega_e\; \mathrm{d}\Omega_\nu \\ &\cdot\; \left(1 + a\;\frac{\mathbf{p}_e\mathbf{p}_\nu}{EE_\nu} + b\;\frac{m_e}{E} + \langle\mathbf{s}_n\rangle\left[A\;\frac{\mathbf{p}_e}{E} + B\;\frac{\mathbf{p}_\nu}{E_\nu} + D\;\frac{\mathbf{p}_e\times\mathbf{p}_\nu}{EE_\nu}\right]\right), \end{aligned} \tag{2.18}$$

where $\mathbf{p}_e$ and $\mathbf{p}_\nu$ are the momenta of electron and anti-neutrino, E and E_ν their energies and $\langle\mathbf{s}_n\rangle$ is the neutron spin. The parameters a, A, B and D are called angular correlation coefficients: a is the correlation between the momenta of electron and neutrino, A is the correlation between neutron spin and electron momentum, and B is the correlation between neutron spin and neutrino momentum. The so called "triple coefficient" D is the correlation between $\mathbf{p}_e$, $\mathbf{p}_\nu$ and $\langle\mathbf{s}_n\rangle$. b is the Fierz interference term, which includes scalar and tensor

type terms, i.e. mixed products of vector and scalar coupling strength $g_S g_V$ and axial and tensor coupling strength $g_T g_A$ (see also subsection 2.1.4). Parity is violated when A and B are nonzero. A non-vanishing coefficient D would violate time reversal invariance.

All coefficients are functions of $\lambda = \frac{g_A}{g_V}$ and assuming V-A-theory, which assumes no scalar and tensor type terms at all, they can be written as

$$a = \frac{1-|\lambda|^2}{1+3|\lambda|^2} \quad A = -2\,\frac{|\lambda|^2 + \mathrm{Re}(\lambda)}{1+3|\lambda|^2} \quad B = 2\,\frac{|\lambda|^2 - \mathrm{Re}(\lambda)}{1+3|\lambda|^2} \quad D = \frac{2\,\mathrm{Im}(\lambda)}{1+3|\lambda|^2}. \tag{2.19}$$

The measured electron asymmetry $A(E)$ in (2.18) is influenced by weak magnetism, proton recoil and $g_A g_V$ interference terms, expressed in a formula given by *Wilkinson* [Wil82]:

$$A(E) = A \cdot (1 - \frac{\delta_R}{A}) \left(1 + A_{wm}\left[A_1 \frac{E_{e,max} + m_e}{m_e} + A_2 \frac{E_e + m_e}{m_e} + A_3 \frac{m_e}{E_e + m_e}\right]\right), \tag{2.20}$$

with

$$\begin{aligned} A_{wm} &= \frac{\lambda + 2\kappa + 1}{\lambda(1-\lambda)(1+3\lambda^2)} \frac{m_e}{m_n} \approx -1.7 \cdot 10^{-3} \\ A_1 &= \lambda^2 - \frac{2}{3}\lambda - \frac{1}{3} \approx 2.1 \\ A_2 &= \lambda^3 - 3\lambda^2 + \frac{5}{3}\lambda + \frac{1}{3} \approx -8.6 \\ A_3 &= 2\lambda^2(1+\lambda) \approx -0.85 \end{aligned} \tag{2.21}$$

The weak magnetism coefficient g_{wm} has to be corrected due to inner radiation, this is accounted for in $\kappa \approx 1.85$ [Bae96]. The electron's kinetic energy is given by E_e, its maximum value by $E_{e,max}$.

2.1.4 Deviations from V-A-Theory

The Fierz-Term: This term, expressed by the coefficient b in formula (2.18), incorporates scalar and tensor terms (g_S and g_T) in the Lagrangian and is therefore equal to zero in the pure V-A-theory. But one can derive expressions for the angular correlation coefficients a, A and B assuming non vanishing scalar and tensor terms. The appearing ratios $\alpha = g_S/g_V$ and $\beta = g_T/g_A$ in this expressions can be calculated for different values of a, A and B, giving restrictions to the admixture of g_T and g_S. These restrictions exclude $\alpha = \beta = 0$ at the level of one standard deviation concerning the experimental data [Yer00]. A new PERKEO III spectrometer is designed to determine correlation coefficients with very high accuracy (see chapter 5). Small effects like the fierz term may be observed with this insrument.

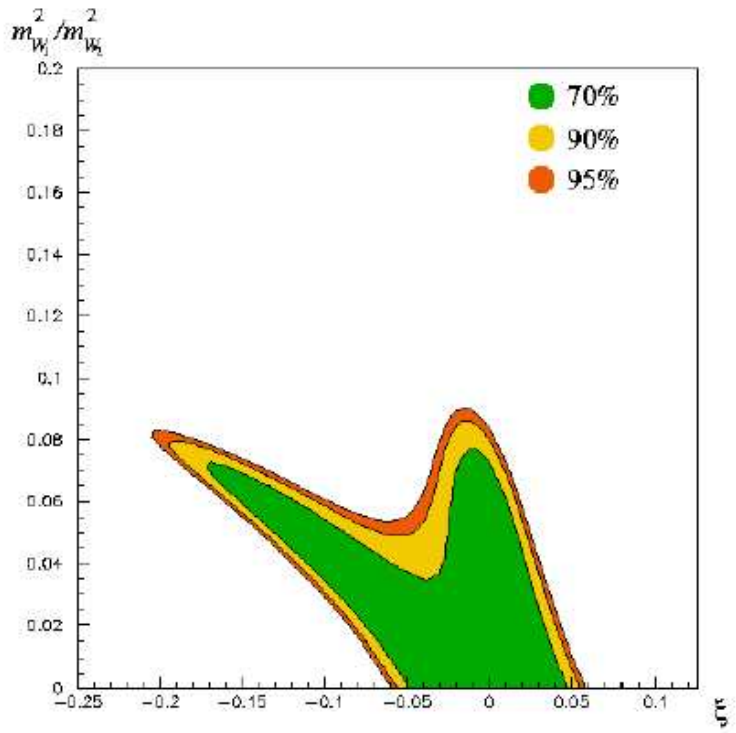

Figure 2.4: Exclusion plot for values of the left-right-symmetric (L-R) model. The coloured regions are allowed with 70 %, 90 %, and 95 % confidence level. On the axis of abscissa the mixing angle ζ is shown, the mass ratio $\delta = \frac{m1}{m2}$ is plotted on the y-axis. Since there are no right handed currents in the Standard Model it corresponds to the point $\delta = \zeta = 0$. [Figure from [Kre04]]

Right-handed Currents: The Standard Model (SM) cannot explain the origin of parity violation observed in weak decays. Some theoretic models extending the SM give reasonable explanations for the violation, like the manifest left-right-symmetric model (L-R model) [Moh75]. It introduces a W_R-boson for the interaction with right-handed particles. Furthermore the bosons are superpositions of the mass eigenstates W_1 and W_2:

$$\begin{pmatrix} W_L \\ W_R \end{pmatrix} = \begin{pmatrix} \cos\zeta & -\sin\zeta \\ e^{i\phi}\sin\zeta & e^{i\phi}\cos\zeta \end{pmatrix} \begin{pmatrix} W_1 \\ W_2 \end{pmatrix}. \tag{2.22}$$

ζ is a mixing angle and ϕ is a CP-violating phase. More free parameters in this model are the ratio of the couplings

$$\lambda = \frac{g_A}{g_V} \quad \text{and} \quad \delta = \frac{m_1^2}{m_2^2}, \tag{2.23}$$

where $m_{1,2}$ are the masses of the bosons $W_{1,2}$.

Parity-violation in this model depends on the ratio δ for $m_1 \ll m_2$ at mixing angles ζ[4]. So in the L-R model all correlation coefficients in (2.19) depend on parameters λ, δ and ζ. Since this thesis covers the measurement of the neutrino asymmetry B we are interested in how B affects the parameters of the L-R model. Certainly the admixture of right-handed bosons is crucially affected by the value of B (the SM includes only left-handed neutrinos) and different values for the neutrino asymmetry would considerably change the allowed δ region. The situation for the current values $A = -0.1173(13)$ and $B = 0.983(4)$ [PDG04] is shown in figure 2.4.

2.2 Measuring the Asymmetry B

In summer 2004 we measured the correlation coefficient between the spin of polarized neutrons and the momentum of the neutrino from neutron decay, the so called neutrino asymmetry B. The measurement was performed with the spectrometer PERKEO II (figure 2.5) located at the beam position PF1b of the *Institut Laue Langevin (ILL)* in Grenoble, France.

PERKEO II features two scintillation detectors each read out by six photomultiplier tubes and a split-pair configuration with a maximum magnetic field of 1.03 T in the center of the spectrometer. The arrangement of the magnetic field enables us to observe two complete hemispheres. In addition we installed thin carbon foils set on high voltage to get an electric field outside the decay volume (i.e. the region in the spectrometer where neutron decays are observed).

The magnetic and electric field lines are arranged perpendicular to the neutron beam. Electrons and protons emitted by neutrons decay in the center of the spectrometer and are guided along the magnetic field lines towards the detectors. The electrons ($E_{max} = 782$ keV) are measured directly with scintillation detectors. The protons are too slow ($E_{p,max} = 780$ eV) and therefore do not deposit enough energy in the scintillator to exceed the energy threshold. Hence we accelerate the protons in the electric field towards the carbon foil. Here they interact with the foil producing secondary electrons which can be detected. In this way we are able to detect electrons and protons emitted in the same hemisphere, which gives rise to a systematically very clean method to determine B (see below). Since we are able to observe two complete hemispheres, we have a full $2 \times 2\pi$ detector. Hence no solid angle corrections have to be applied.

Two supermirror polarizers arranged in crossed geometry [**?**] polarize the neutrons with an efficiency of about 99.7 %[5][Schu04]. A radiofrequency spinflipper allows us to turn the neutron spin by 180°.

[4]Since there is no W_R in the SM, there is no mixing, which yields an infinite W_2 mass. Therefore the SM is included in the exclusion plot at the point $\delta = \zeta = 0$.

[5]The improvement of the polarization crucially decreased the systematic error!

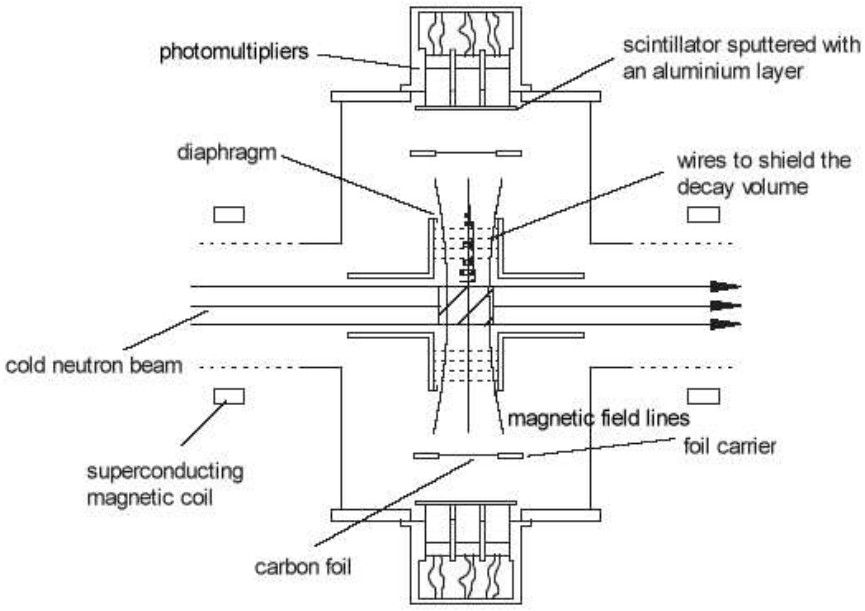

Figure 2.5: The spectrometer PERKEO II for the the measurement of the neutrino asymmetry B. Neutron decays outside the decay volume are screened by diaphragms. Inside electrons and protons are guided by the magnetic field lines to the detectors. In this was all charged particles are detected and we obtain a $2 \times 2\pi$ detector.

Combined electron-proton spectra: One can combine the electron-proton spectrum in two ways: Either both particles are emitted into the same hemisphere or into different hemispheres. The number of particles detected in the same hemisphere is denoted by $N^{\uparrow\uparrow}$, emission in opposite directions by $N^{\uparrow\downarrow}$. The first arrow indicates the electron's heading, the emission direction of the proton is given by the second arrow. If the arrow points upward, the heading of the decay product is aligned with the direction of the neutron spin.

For each combination we get an asymmetry,

$$B^1_{exp} = \frac{N^{\downarrow\downarrow} - N^{\uparrow\uparrow}}{N^{\downarrow\downarrow} + N^{\uparrow\uparrow}} \quad \text{(same hemisphere)}, \tag{2.24}$$

$$B^2_{exp} = \frac{N^{\uparrow\downarrow} - N^{\uparrow\downarrow}}{N^{\uparrow\downarrow} + N^{\uparrow\downarrow}} \quad \text{(opposite hemisphere)}. \tag{2.25}$$

The analytical expression of B^1_{exp} with a beam polarization P (we assume a flipping efficiency of 100 % in this expression) is given by [Kre04]:

$$\begin{aligned} B^1_{exp} &= \frac{2PA\beta(\frac{r}{3} - \frac{1}{2}) + PB(1 - \frac{r^2}{3})}{2 - r + \frac{\alpha\beta}{2}(\frac{r^2}{2} - 1)} \quad \text{for} \quad r < 1 \\ B^1_{exp} &= \frac{2PB\frac{1}{3r} - PA\beta\frac{1}{3r^2}}{\frac{1}{r} - \alpha\beta\frac{1}{4r^2}} \quad \text{for} \quad r > 1, \end{aligned} \tag{2.26}$$

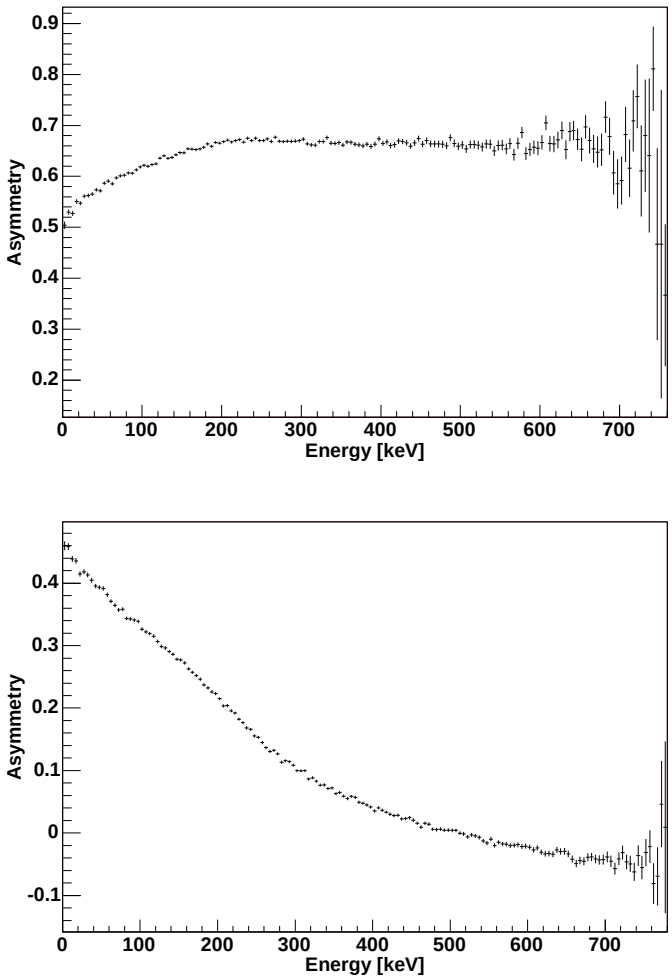

Figure 2.6: Monte Carlo simulation of the neutrino asymmetries without any experimental corrections: The asymmetry B^1, where electron and proton are measured in the same hemisphere, is shown in the upper figure. The neutrino asymmetry B^2 for electron and proton measured in opposite hemispheres is shown below. The abscissa denotes the electron's kinetic energy.

where a, A, and B are the angular correlation coefficients (see 2.18), $\beta = \frac{v}{c}$, and r is an energy dependent factor defined by $r = \beta\frac{E_e}{E_\nu}$. E_e and E_ν correspond to the kinetic energy of the electron and the neutrino. Compared to B^2, the asymmetry B^1 measured the same hemisphere has a smaller dependence on the electron energy and a higher sensitivity to B [Rei99] (see also figure 2.6).

Chapter 3

Experimental Realization

In summer 2004 we did the measurement to determine the neutrino-asymmetry B at the *Institut Laue Langevin* (ILL) in Grenoble which operates the most intense cold neutron[1] source in the world[2].

The overall setup of the experiment is shown in figure 3.1. The neutrons first pass two supermirror polarizers, a spin flipper, and are guided through a collimation system. The beam enters the spectrometer and finally reaches the beamstop.

Our aim was to determine the neutrino asymmetry B with a smaller error than the previous experiment which was performed with PERKEO II in 2001 ([Kre05a], error: 1.2 %). This chapter describes

- technical improvements and add-ons to the setup compared to the experiment performed in 2000.
- alignment of the neutron beam with the magnetic field of the spectrometer PERKEO II, done with the so-called B-n-scans. Here B denotes the magnetic field and n neutron.
- the operation of a scanner used for calibration of the scintillation detectors
- the measurement of protons with a high voltage setup effects observed in our experiment due to strong electric fields.

Coordinate system: In this thesis, we use the following coordinate system:

x	axis runs through the centers of the coils
y	axis follows the beamline
z	axis defines the vertical direction .

[1] Cold neutrons have a kinetic energy of about 2 meV.
[2] We measured the proton asymmetry C at the same time.

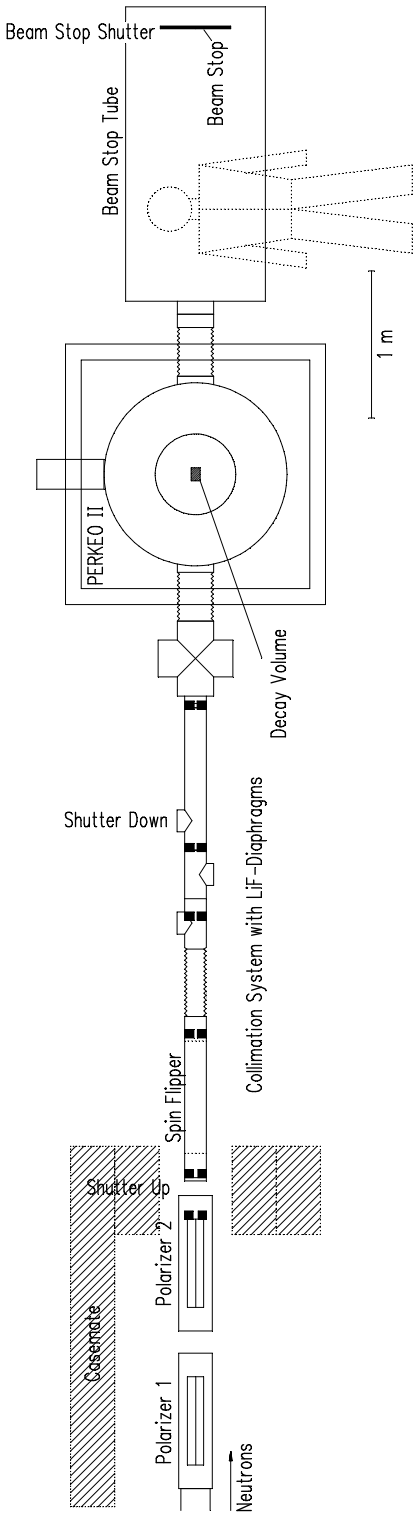

Figure 3.1: Beamline and spectrometer PERKEO II located at beam position PF1b at the ILL. Systematic improvements were made compared to the experiment performed in 2000 by using two supermirror polarizers and an improved Data acquisition system.

3.1 Improvements and Add-ons to the Setup

Compared to the measurement of the asymmetry B performed in 2000 [Kre04] the experimental setup has been improved at several points: The beamline was modified using additional instruments like a second supermirror polarizer and a new spinflipper. Furthermore the high voltage setup inside the spectrometer was upgraded and the data acquisition system was improved.

3.1.1 The Beamline

Supermirror Polarizers: The beamline shown in figure 3.1 offers important new features. In the experiment we used two new supermirror polarizers (instead of one) in a crossed geometry [Kre05b]. As a consequence the beam polarization changed from 98.14(2) % between 3.2 and 13.0 Å [Rei99] to 99.7(1) % between 2 and 12 Å [Kre05b].

Spinflipper: The radio frequency spinflipper is used to turn the spin of the neutrons periodically by 180. The flipping efficiency was almost 100%.

The Beamstop: Neutrons reaching the end of the beamstop are absorbed by ^{6}Li[3] but also scattered. To prevent that scattered neutrons reach the spectrometer, we installed a cage made out of neutron absorbing material inside the beamstop: The side towards the spectrometer was made out of borated glass, the side walls were made out of `Boral`, a boron-aluminium alloy. The reaction of neutrons with boron yields a γ-background that can be shielded efficiently with lead [Krem04].

The vacuum: Since neutrons, electrons, and protons should not scatter on atoms of the air a good vacuum is mandatory. To reach this, we used a small 300 $\frac{\ell}{sec}$ `Alcatel` turbopump to evacuate the beamline and an `Ebara ICP200U` cryopump[4] (pumping speed: 1500 $\frac{\ell}{sec}$ for N_2) installed just in front of PERKEO II. Two `Leybold TURBOVAC 1500` pumps with an exhaustion rate of 1500 $\frac{\ell}{sec}$ each were assembled at the beamstop. The averaged vacuum was about $1 \cdot 10^{-6}$ mbar, the best value we achieved was $3.6 \cdot 10^{-7}$ mbar measured at the beamstop.

[3] In the reaction Li+n many fast neutrons (energies of fast neutrons are higher than 1 MeV) are also generated and may react with the hydrogen of the scintillators. One has to moderate and to remove these neutrons since they produce a crucial background.

[4] This pump improved our vacuum only by a factor of two since it was not running properly.

3.1.2 Data Acquisition

The data acquisition system converts the analog signals of the photomultiplier tubes to digital data (via ADCs (Analog to Digital Converters)) and transfers this data together with other digital information (e.g. timing information) to the computer.

Afterpulses: Tests showed that the photomultiplier tubes have an certain probability to produce a coincident afterpulse within 10 μs after an event [Schu05]. An afterpulse cannot be distinguished from a proton or electron signal and can therefore be interpreted as such a signal. This effect made the correct identification of signals quite difficult in the experiment of 2001. To avoid this we used a special condition for a proton/electron signal: For a valid event, at least two out of six photomultipliers have to give a signal. In this way the proton detection efficiency decreases, but we avoid an afterpulse correction to our proton spectra.

Accidential coincidences and Backgound Stops: We avoided problems due to accidential coincidences and background (i.e. stops that are not due to protons) in two ways:

- We measured up to 32 stop signals with a TDC (Time to Digital Converter)[5]. The slowest protons have reached the detector after time t_{max}. Therefore, all signals measured after t_{max} have to be accidential coincidences (background signals). Hence we can measure the accidential coincidences with this delayed coincidence method and subtract the effect from the spectra.
- If one measures only one stop signal, a proton stop would eventually suppress stops due to background events and the other way round. Since we measure up to 32 stops we ensure that we measure the proton and the full background which is important to subtract the background from the signal.

3.1.3 High Voltage Setup

Protons emitted in neutron decay have a maximum kinetic energy of $E_{p,max} = 780$ eV. Compared to the highest electron energy, $E_{e,max} = 782$ keV, the proton energy is three orders of magnitude smaller. It is much too small to be detectable in our scintillation detectors. Therefore the protons have to be accelerated in a high electric field where they gain energy in the keV range. Thin carbon foils (with a maximum thickness of 40 μg/cm^2

[5]The first signal (electron) starts a coincidence window of 80 μs. The coincidence time of up to 32 stop events (protons and background) within this window is measured and the energy of the first four stops is taken.

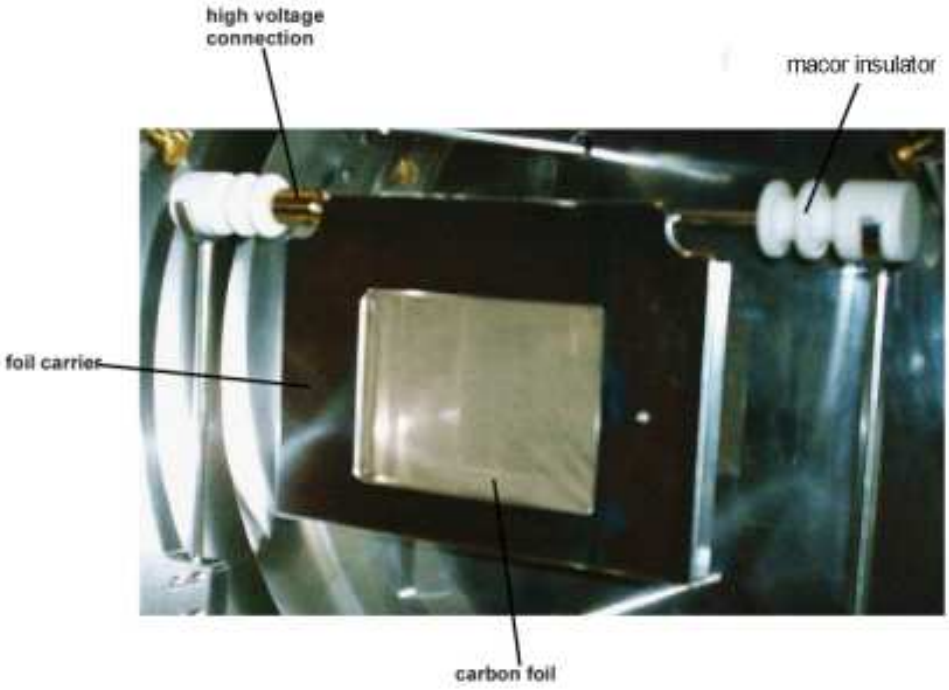

Figure 3.2: This picture shows the carbon foil installed in PERKEO II. The foil and the carrier are set on high voltage. The carrier is polished to avoid field emission on spikes which may yield background signals.

[Rei99]) are placed between the decay volume and the detectors (figure 2.5 and 3.2) and set on high negative potential ($U = -18$ kV). Protons are accelerated towards the foil and produce several secondary electrons due to interaction with the foil. These electrons depose detectable energy. Since the scintillation detectors have an energy threshold of approximately 35 keV [Schu05], we want to have an electric field as high as possible to be sensitive to even low energy protons (one proton generates several 18 keV-electrons, so the overall signal is obove the threshold).

Since all other parts of the spectrometer are grounded, we have to ensure that all parts on which electric field lines may end, do not show spikes or sharp edges. Spikes would cause very high fields leading to disturbing effects like field emissions. Therefore we made much effort to remove edges and to polish the surface of all relevant parts. This is especially important for the carrier of the foil, figure 3.2.

Furthermore we have to ensure that no electric field is present in the decay volume since the positive/negative acceleration of the decay products would change the asymmetry. We arranged four grids made out of aluminium wires in intervals of 20 mm to shield the center of the spectrometer (figure 2.5). The gap between the wires of the grids was 6 mm. We used aluminium wires since a test showed that aluminium wires give less background at

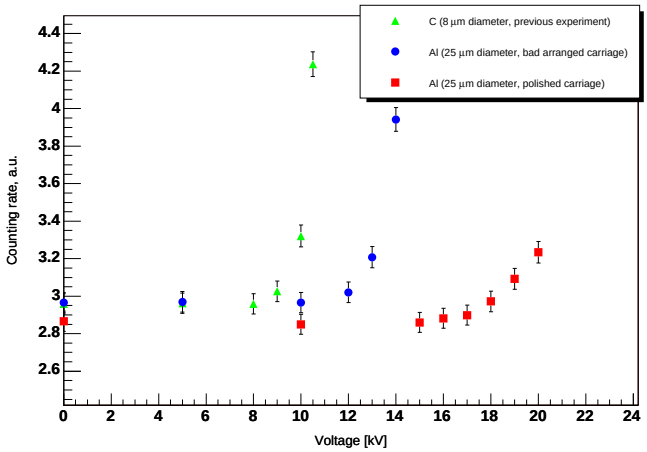

Figure 3.3: High voltage effects: Different wire materials and diameters cause significantly different signals. Since the 25 μm aluminium wires (red squares) result in the lowest background signals even at high voltages we used this material in our experimental configuration [Schu05].

high voltages compared to the carbon wires used before (figure 3.3). Wires with a diameter of 10 μm and 25 μm (instead of 8 μm carbon wires used 2001) were chosen because we wanted to avoid the very high fields arising at small diameters [Schu05]. As a negative side effect larger wires should give rise to a higher absorption and scattering rate of protons and electrons. This so-called grid-effect is under examination.

3.2 Alignment of the Neutron Beam to the B-field

The magnetic field of PERKEO II is generated by two superconducting coils arranged in a split pair configuration producing a field maximum between the coils: A small gradient leads to lower field strengths outside the center. It is necessary to align the center of the neutron beam with the maximum of the magnetic field. Otherwise the measured asymmetry is changed due to the magnetic mirror effect.

This effect is called mirror effect since electrons and protons can be reflected when following a rising B-field gradient. The reflection probability of a charged particle depends on the magnetic field strength B_0 at the point of the emission of the particle, i.e. at the place the neutron decays, the maximum of the field B_{max} and on the angle θ between the direction of emission and the field line direction. We define the critical angle

$$\theta_{crit} = \arcsin\sqrt{\frac{B_0}{B_{max}}} \; . \tag{3.1}$$

If $\theta > \theta_{crit}$ the condition of reflection is fullfilled. A symmetric neutron distribution around the field maximum is required to achieve the same θ_{crit} on both sides of B_{max} to reduce systematic effects.

The mirror effect changes the neutrino asymmetry B, but for narrow beams the relative change of the asymmetry $\widetilde{B}_{mm}$ (mm denotes magnetic mirror) is smaller. Hence we in-

stalled a diaphragm about 1.5 m in front of the spectrometer, which reduced the width of the neutron beam to 50 mm. In the electron energy region of 200-400 keV a beam width of about 80 mm yields $\widetilde{B}_{mm} \approx -0.75\%$, whereas a width of 50 mm gives $\widetilde{B}_{mm} \approx -0.37\%$ [Rei99]. Of course an even smaller beam would reduce the change in B even more, but one also looses statistics and we therefore had to make a compromise between the two effects.

3.2.1 Position of the B-field

To align the neutron beam with the magnetic field, we first determined the position of the magnetic field maximum. As a reference point we used a laser beam aligned parallel to the neutron beam passing the spectrometer and pointing always at a fixed target. The measurement of the B-field was done with a gaussmeter[6] (a Hall-effect probe) moving in three directions. We fixed the y and z positions at the center of the decay volume and moved the probe along the x axis. Measuring the B-field in this way gives the shape of the field inside the detector as shown in figure 3.4. The laser defined the point $x = 0$. Afterwards we went to different z and y positions and repeated the measurement. We found a displacement

[6]Gaussmeter 9900 Series of `F. W. Bell`

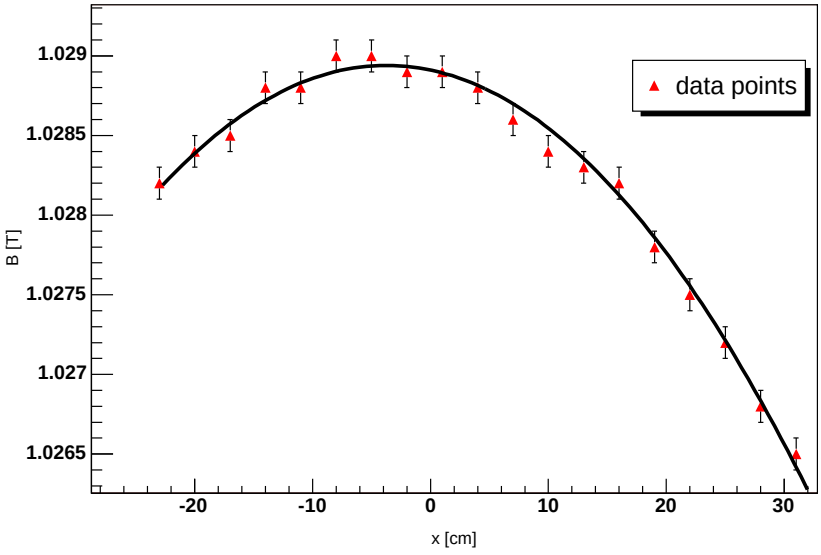

Figure 3.4: The figure shows the absolute values of the magnetic field measured at different x positions and for constant y and z positions. This kind of measurement was done also for different z and y values. We found the B-field maximum in x-direction to be located (5.8 ± 1.0) mm next to the laser reference point.

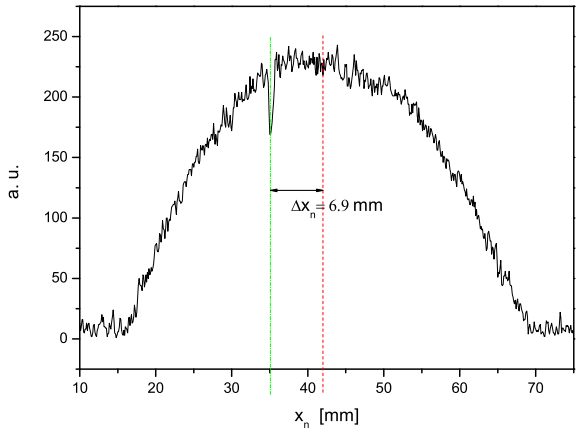

Figure 3.5: Data from the copper foil activation analysis. Cut along the x axis through the neutron beam in the center of the decay volume. Δx_n is the displacement of the beam center (red line) relative to the laser reference point (green line).

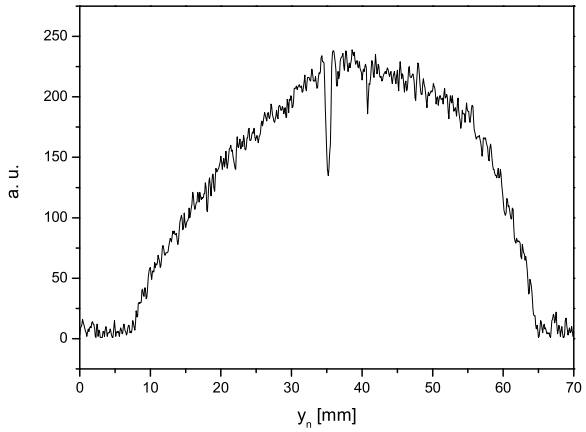

Figure 3.6: Data from the copper foil activation analysis. The height of the beam along the z axis, measured in the center of the spectrometer.

between the laserbeam and the magnetic field maximum of $\triangle x_B = (5.8 \pm 1.0)$ mm. The error is caused by systematics, since we could neither define the position of the gaussmeter nor the position of the laser beam with higher accuracy (the laser dot was too big; in future experiments maybe a more precise determination of the relative positions could be done with a theodolite).

The next step was to determine the neutron beam position with respect to the laser reference point.

3.2.2 Neutron Beam Alignment

The displacement between the reference point ($x = 0$) and the B-field maximum $\triangle x_B$ had to be compared with the relative position of the neutron beam $\triangle x_n$. We determined

$\triangle x_n$ by using the copper foil activation analysis method, i.e. placing copper foils in the neutron beam. Natural copper consists of 69.2% ^{63}Cu and 30.8% ^{65}Cu. Neutrons activate these isotopes and produce ^{64}Cu and ^{66}Cu. The activated copper decays with a lifetime of $\tau(^{64}Cu) = 18.3$ h and $\tau(^{66}Cu) = 7.39$ min. One finally measures the decay of the long living isotope by using a radiation sensitive imageplate that can be read out with a suitable scanner[7]. The procedure of activation and readout is linear to the thickness and density of the foil used and to the neutron capture flux[8] ϕ_c [Krem04]. Assuming a constant neutron flux and choosing always the same irradiation time ($t_{irr} = 45$ min), identical conditions for the activation of the imageplate ($t_{image} = 20$ min) and the readout (the scanning resolution was 100 μm), this is an excellent method to determine the shape of a neutron beam (figure 3.7).

We optimized the shape of the beam in several steps by adjusting the last diaphragm of the beamline. Finally the neutron beam had a width of $x_{beam} \approx 52$ mm and a height of $z_{beam} \approx 58$ mm, as can be seen in figures 3.5 and 3.6. The big dip in the figures is caused by a hole in the copper foil, that indicates the laser reference point. Its displacement relative to the mean of the neutron beam is $\triangle x_n = (6.9 \pm 1.0)$ mm. The systematic error again arises from the big laser spot on the copper foil. Comparing this value with the position of the magnetic field maximum we get a displacement D_x of the neutron beam relative to the B-field maximum of

$$D_x = \triangle x_n - \triangle x_B = (6.9 \pm 1.0)\text{ mm} - (5.8 \pm 1.0)\text{ mm} = (1.1 \pm 1.4)\text{ mm}. \tag{3.2}$$

Within the errors we have no displacement. Therefore corrections due to an asymmetric beam distribution around the magnetic field maximum can be neglected.

3.3 Calibration of the Detectors

The detection of the β-decay electrons and secondary electrons was done using two scintillators each read out by six photomultiplier tubes.

We used a 5 mm thick scintillator (`Bicron BC 404`) glued with optical cement (`BC 600`) to a light guide (`BC 810`) with a thickness of 30 mm and a dimension of 9×13 cm^2. Scintillator and light guide have the same refraction coefficient to avoid light losses at the contact surface due to refraction and total reflection. We covered the fringes of the detectors with a special paint (`BC 620`) that isotropically scatters incident photons to increase the number of photons reaching the photomultipliers. Finally the free side of the scintillator (the side

[7] 'STORM 820' by `Molecular Dynamics`

[8] The capture flux ϕ_c is defined via

$$\phi_c = \int_v \phi(v)\frac{v_0}{v}\mathrm{d}v,$$

where ϕ is the absolute flux, v the neutron velocity and $v_0 = 2200$ m s^{-1} the thermal velocity.

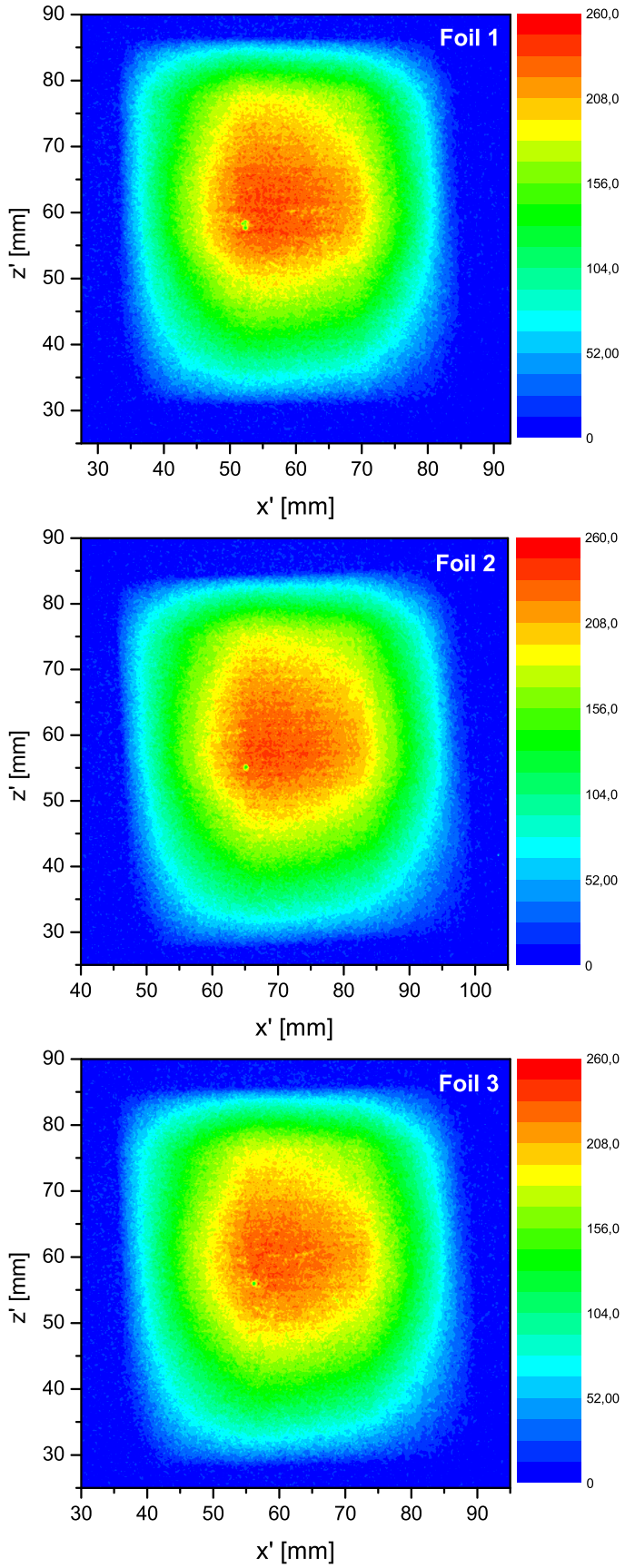

Figure 3.7: The figures show the shape of the neutron beam for different y-positions along the neutron beam obtained via copper foil activation analysis. 'Foil 1' defines the beginning of the decay volume, i.e. the reactor side of the decay volume. The shape of the beam in the center of the decay volume is shown in figure 'Foil 2', placed about 54 mm behind 'Foil 1'. The last foil was placed at the beamstop side, approximately 35 mm behind the second foil.
From the figures we conclude that the beam is homogeneous over the decay volume. Therefore we can assume a constant magnetic mirror effect over the whole length of the decay volume. (Note: The coordinates of the figures are relative coordinates that are not perfectly synchronized.)

"seeing" the particles) was sputtered with a very thin aluminium layer ($d \approx 30$ nm) to ground the detectors.

On the back side, six `Hamamatsu` photomultipliers were arranged in a special setup to achieve an optimal covering of the lightguide surface [Plo00]. Good contact between lightguide and photomultiplier was obtained by using vacuum grease (`Varian`).

The detector area of 117 cm^2 is quite large. Therefore we built a scanner (figure 3.8) to determine the detector function, which should be as homogeneous as possible [Bre03]. The principle of testing the homogeneity of the detector is the following:
We used a point like bismuth ^{207}Bi source[9] emitting electrons of two well defined energies ($E_e = 504.5$ keV and $E_e = 996.9$ keV) and placed it inside the spectrometer. The emitted electrons are guided by the magnetic field to a certain position on the scintillator and we get a position dependent detector signal. Moving the source to different points, we can measure the energy deposited at arbitrary spots on the scintillator.

However, we have to consider the gyration of the electrons around the magnetic field lines. This causes an uncertainty in defining the exact position at which the electrons hit the scintillator. The gyration radius R_{Gyr} can be calculated by assuming the B-field to be parallel to the E-field (which is nearly the case in PERKEO II) and we get [Jac02]

$$R_{Gyr} = \frac{p_t}{300B}. \tag{3.3}$$

The maximum value $R_{Gyr,max}$ is realised with the maximum electron momentum $p_{t,max}$ transversal to the field lines at low B-field values. For neutron decay we get $p_{t,max} = 1.187$ MeV/c and a B-field strength of about $B = 0.69$ T near the detectors, yielding a gyration radius of $R_{Gyr,max} = 5.7$ mm[10]. The points on the scintillator are therefore small enough to obtain a position sensitive detector function.

3.3.1 The Scanner used for Calibration

The scanner is shown in figure 3.8. It must be able to move the calibration source in y and z direction so that we can scan the whole scintillator. All components of the scanner have to work in a high magnetic field, a condition that also the motors have to fullfill: We therefore used piezo motors [Bre03]. To get the position of the source a potentiometer at each axis was used. In y direction the potentiometer was turned by a cogwheel running along a toothed bar; here no problems occured in reaching the target positions.

The movement along the z axis caused some problems within the vacuum. The piezo motor turned a wheel (which was connected to a potentiometer) that coiled a thin plastic string.

[9] A ^{139}Ce source ($E_e = 136.6$ keV was used in a second scan.)

[10] The curvature and gradient drifts caused by the inhomogenious magnetic field are neglectable since the curvature drift yields a displacement of about 1 mm at the scintillators, the gradient drift is even smaller [Schu04].

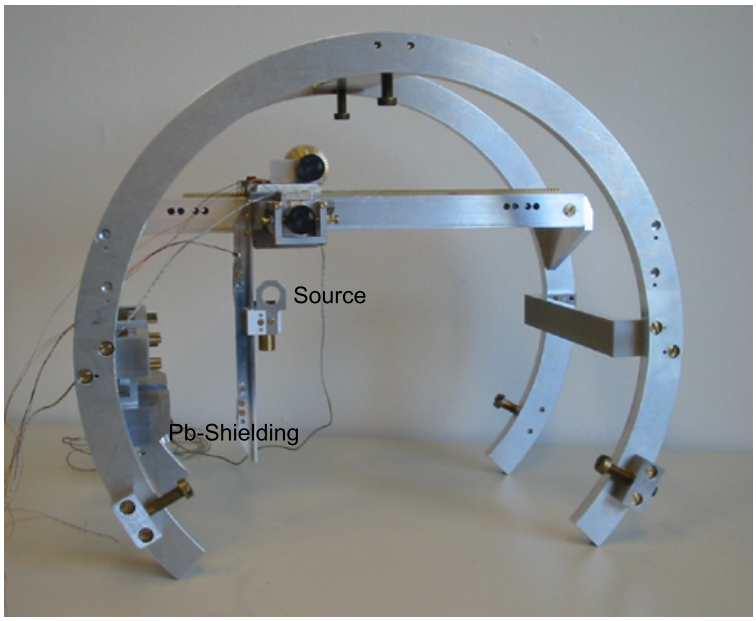

Figure 3.8: The scanner used in the experiment. The calibration source fixed at the white dice can be moved in y and z direction to scan the whole detector.

The free end of the string was connected to a dice with the source movable on a bar along z direction. In the evacuated spectrometer problems occured due to friction between the bar and the dice and the string falling of the wheel. Therefore we had some difficulties to reach a target position (it turned out that lowering the dice was more problematic, so we began the scans at the lowest z position and moved upwards). Although we solved these difficulties (chapter 3.3.2), an alternative construction of the device for the z direction should be considered for duture measurements. Due to the problems mentioned one should try to construct a device that can lower the probe without using gravitation.

3.3.2 Software Logic

The control software of the scanner should allow the user to reach a given position with high accuracy and as fast as possible. To achieve this we used both possible drive-modes of the piezo motors: the jump-mode and the step-mode. Using jump-mode means that the motor drives on continuously, whereas the step mode moves the motor only step by step, with a minimum stepsize of approximately 0.1 mm. In both cases, the velocity depends on the applied control voltage.

When the user has defined the target positions, the control software starts with determining the distance between the actual position and the position of the first target. The calculated distance defines which drive-mode will be used: Either jump-mode, if the distance is large, or step-mode for short distances. The control voltage is applied for a split of a second and

the new position is read out. This scheme is iterated until the target position is reached. After having reached the target position and having finished the measurement, the source is steered to the next position.

However, as noted above, using these motors in the evacuated spectrometer caused some problems. Therefore we implemented aborts: The program stops trying to get to the target position in case it was not reached after a defined number of attempts and starts moving the probe to the next defined position. Without these aborts the automatic steering to a target position could last for an exorbitant long time.

A detailed pseudo-code of the algorithm described above can be found in the appendix.

3.4 High Voltage

After having installed the setup (the aluminium wires, the carbon foils, and the detectors) inside the spectrometer, we applied high voltage to the carbon foils step by step and checked its influence on the event count rates. The tests were performed with a vacuum of around $3 - 5 \cdot 10^{-6}$ mbar.

The voltage was applied in two different ways:

- One foil was set on high voltage while the other foil was grounded
- The high voltage was simultaneously applied to both foils.

High voltage on one foil, the other one grounded: We found a smaller count rate of the detector at the grounded side compared to the other detector. This is caused by the fact, that the detector with the foil on high voltage is shielded by the electric field since negatively charged particles have to get over the potential barrier. In case they do not have enough energy, they are reflected and guided to the opposite detector.

Positively charged particles accelerated towards the foil may produce secondary electrons. But since these electrons are emitted in all directions they will not cause an asymmetric count rate.

These tests should show the same count rate at the grounded foils and on the foil on high voltage, regardless which foil was grounded. But since we found different count rates, we assume that foil 1 (on detector 1 side) emitted much more particles producing a higher background.

Applying voltage to both foils: While simultaneously applying voltage to both foils, the voltage supply of the photomultiplier tubes was shut-off automatically from time to time. This emergency shut-off is initialized if the current in one of the photomultiplier

tubes is too high. Since a high photomultiplier tube current is equivalent to a high number of detected photons, we assume that electrostatic discharges inside PERKEO II initialized these shut-offs. This was confirmed by installing an amperemeter and measuring discharge currents, followed by emergency shut-offs.

Again we measured a higher count rate at foil 1, compared to the rate on side 2. To get rid of the discharge currents we installed an aluminium cuboid at the top of the carrier of foil 1: This slightly changes the electric field lines above the foil and should avoid an accumulation of charged particles by guiding them out of the inner part of the setup. In this way the discharge currents causing the emergency shut-offs disappeard, but still a high, sometimes instable count rate was measured at foil 1 (figure 3.9).

In order to find out the origin and to eliminate this effect we inspected and changed several components of the setup:

- **The foil:** We replaced the foil, we turned the foil, but the effect did not vanish.
- **The detector:** The high count of detector 1 was mainly caused by two photomultiplier tubes which covered the beamstop-side of the detector. Hence we turned the detector by 180. Now the other photomultiplier tubes on the beamstop-side showed the high count rate, which excludes an effect due to the detector itself.
- **The aluminium wires** to shield the decay volume were checked and some of them replaced. The result was slightly better but still not satisfactory.
- **High voltage supply:** We installed the contact of the high voltage supply (see figure 3.2) on the opposite side of the foil. This had no effect either.

The high voltage setup was identical for both detectors, only the foils differed. Therefore all tests described indicate that the high count rate at foil 1 side was generated by the foil itself.

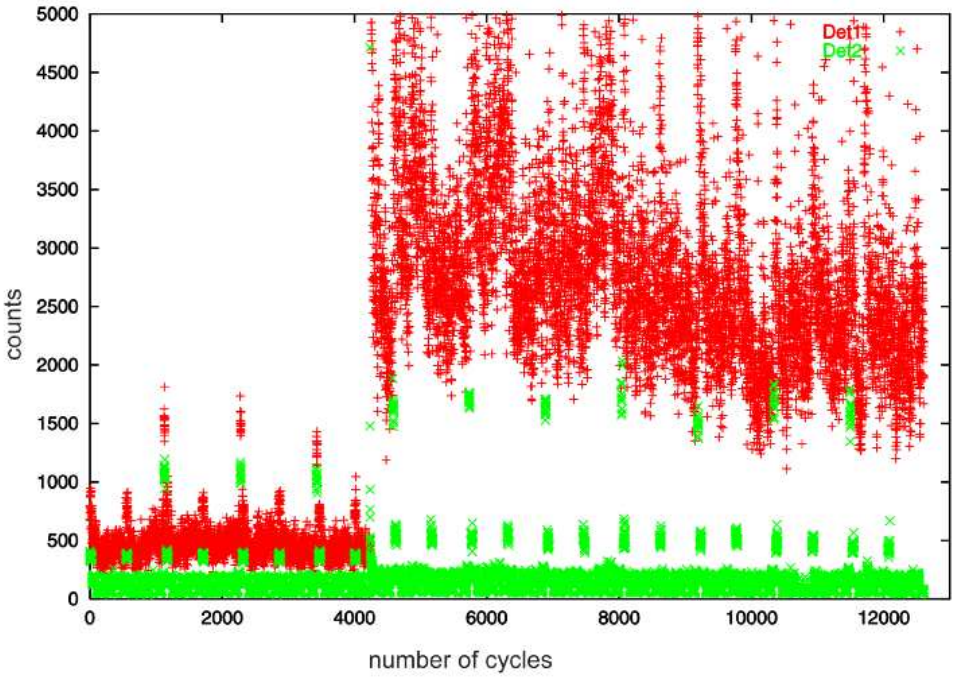

Figure 3.9: High voltage effects: The event count rate for both detectors. The abscissa indicates the number of measured cycles (a cycle lasts for 2 seconds), the number of events is shown on the ordinate. The periodic rise of the counts is caused by the calibration sources. The sudden boost of the count rate after cycle 4000 is probably due to a discharge current. The count rate for detector 1 is always higher, also before the boost.

Chapter 4

Monte Carlo Simulations for PERKEO II

A simulation of neutron decay inside the spectrometer PERKEO II helps to examine systematic effects. Furthermore, a better understanding of background phenomena may be obtained. This chapter describes a program that simulates spectra considering systematic effects and presents corrections on the measured spectra due to these effects.

4.1 Principle of Monte Carlo Simulation

Monte Carlo Simulations are a commonly used tool in experimental physics: The program written in this thesis simulates an experiment performed with ideal conditions, systematic effects may be considered or discounted optionally.
There are different methods to simulate a given problem with the Monte Carlo technique: The one used in the program described below is called the acceptance-rejection or von Neumann method: The probability density function $f(x)$ for a given interval $[a, b]$ is well known. A random number generater defines a value x of the intervall on the abscissa and a value y on the ordinate. If $y \leq f(x)$, x is accepted, otherwise it is rejected and another random value generated (figure 4.1). In this way the accepted x are weighted with the function $f(x)$.

4.2 The program `MoCAsSiN`

The program `MonteCarloAsymmetrySimulation` for `Neutron-Decay` (`MoCAsSiN`), written C++, is based on the Fortran `betasim` code [Rein91] and [Rei99].
The original Fortran code was extended crucially: In addition to the simulation of neutron β-decay, we implemented the following features which describe the specific experimental environment of PERKEO II:

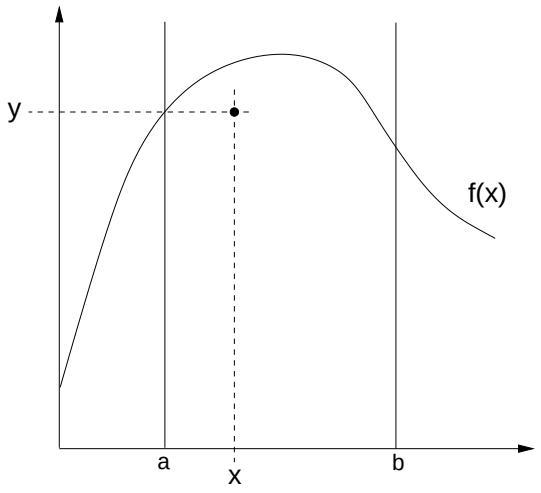

Figure 4.1: Sketch of the acceptance-rejection method: Two values x and y are randomly generated. If $y \leq f(x)$ the value x is accepted. Otherwise a new number is generated.

- **Decay Volume:** The neutron distribution along the x axis (detector to detector) is modelled as realistic as possible. It is again calculated with a Monte Carlo method using the neutron distribution obtained obtained by B-n-scans (chapter 3).

- **Magnetic Mirror Effect:** Charged Particles may be reflected due to an increasing gradient of the magnetic field (see also 3.2) of PERKEO II. The field used in the simulation was obtained by measurements. The correction on the asymmetry B^1 is less 0.04 % due to this effect, there is no correction on B^2. See chapter 4.2.2 for details.

- **Electric Mirror Effect:** The electric mirror effect describes the reflection of charged particles at the electric potential of the carbon foils (chapter 4.2.3). In the region of interest, this effect does not affect the measured spectra.

- **Edge Effect:** The edge effect (chapter 4.2.1) causes changes of the electron spectrum due to the finite decay volume length: Particles from neutron decays at the end of the decay volume may be absorbed by the diaphragms defining its length. The electron spectrum maximally changes by about 10 % at $E_e \approx 600$ keV, in case electron and proton are emitted into the same hemisphere.

- **Time of Flight Spectrum:** We implemented a function to determine the time of flight spectrum of nonrelativistic particles inside the spectrometer. This can be used to analyze the experimental background which is shown in chapter 4.2.4.

- **Detector Function:** The detector function describes the statistical variation of the measured energy. The variations are considered in two steps: First we treat the conversion of photons into electrons inside the photomultiplier tubes. The resulting number of electrons is assumed to be Poisson distributed. Afterwards the electronics broaden the electron current by a Gaussian distribution.

- **Trigger Function:** The detection efficiency depends on the energy deposed in the detector system. Since the data acquisition system is less sensitive to events of low energy, these are detected with a smaller probability than events at higher energies. This energy dependent probability distribution is available in the simulation.

We will discuss some of these topics in detail in the following sections:

4.2.1 The Edge Effect

The decay length that can be observed by the detectors is limited. To obtain a properly defined decay volume length in y direction, we installed diaphragms to shield the products from decays occuring outside the decay volume. Particles emitted at the endings of the volume can be scattered or absorbed by these diaphragms. Due to the gyration around the magnetic field lines, this effect is also relevant for particles moving at some distance of the edge.

The probability for absorption depends on the emission direction with respect to the magnetic field lines and therefore on the particle energy. Since energy and angular distributions for electrons and protons are related (see 2.18), we cannot calculate the edge effect analytically but have to simulate it.

To determine the effect we assume that every particle hitting the diaphragms is absorbed. This assumption is fullfilled with a good approximation [Kre04] since

- all protons are entirely absorbed due to their low energy

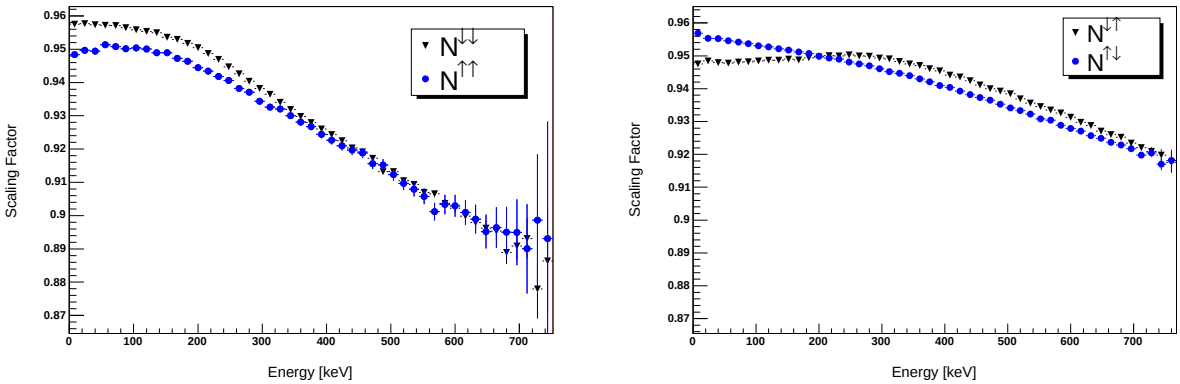

Figure 4.2: Edge Effect: The theoretical spectra (i.e. without edge effect) must be multiplied by the appropriate histograms considering the edge effect. If either the electron or the proton emerging in the decay is absorbed, both particles are lost for the measurement. The left figure shows events in the same hemisphere, on the right the edge effect is given for events in opposite hemispheres.

- for electrons, the probability of a single reflection is about 10 % and of a double reflection about 0.1 % [Leo94]

- the electrons will hit the diaphragms twice in most cases since they gyrate with a rather small slope compared to the length of the diaphragms.

In order to simulate the edge effect, we have to consider the displacement of the gyration center (figure 4.3): The center is not always given by the position of decay. In fact we must consider the azimuth angle ϕ defining the direction of the particle's momentum $\mathbf{p}_\phi$ on a plane perpendiculer to the magnetic field lines. ϕ is determined in the neutron decay. The gyration center is determined by placing the vector $\mathbf{r}_{gyr}$ ($|\mathbf{r}_{gyr}|$ = gyration radius) perpendicular to $\mathbf{p}_\phi$. $\mathbf{r}_{gyr}$ then points to the center around which the particle rotates. Due to the displacement of the center, even particles with a distance to the diaphragm of two gyration radii can be absorbed.

Figure 4.2 shows the quotient of the spectra simulated with and without edge effect. As expected, the effect is larger at higher energies since the gyration radii are larger compared to lower energies. The emission of electron and proton in the same hemisphere results in a big angle between the momenta of the particles (see figure 4.7). In case particles are emitted in opposite hemispheres, their angle relative to the magnetic field lines is smaller. This results in smaller gyration radii. Therefore the edge effect affects the spectra of electron and proton measured in the same hemisphere more than the spectra of particles emitted into opposite directions.

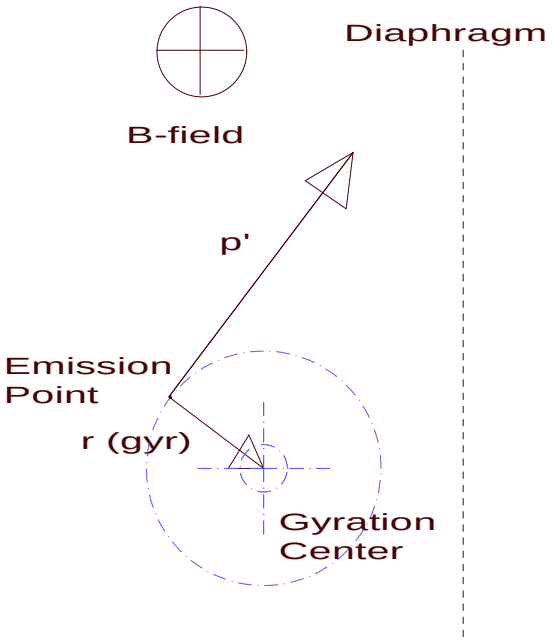

Figure 4.3: Edge Effect: Displacement of the gyration center of a particle due to the emission direction. Shown is a plane perpendicular to the magnetic field lines.
Because of this effect, particles with a distance of up to 2 r_{gyr} can be absorbed by the diaphragms depending on their initial momentum.

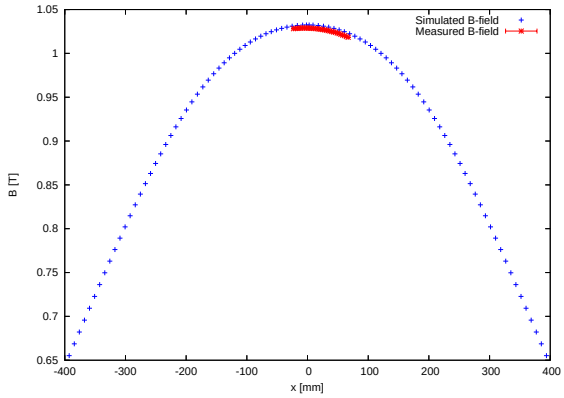

Figure 4.4: Comparison between simulated [Mae05] and measured magnetic field along x for $y = z = 0$ inside PERKEO II. The simulation is plotted over the distance between both detectors (blue crosses). We measured the B-field in the decay volume (red stars). The difference of the maximum is about 0.3 %.

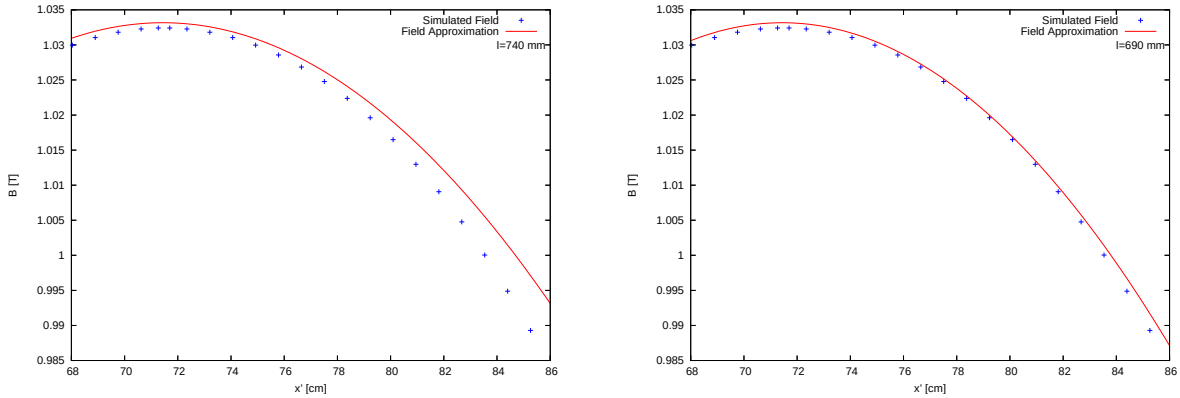

Figure 4.5: The magnetic field inside PERKEO II: x' denotes a relative position. The field approximation (4.1) is very sensitive to the parameter l. To calculate the edge effect a good approximation of the field is needed both in the decay volume and at the position of the diaphragms. $l = 690$ mm (right figure) fullfills this condition much better than the formerly used value $l = 740$ mm ([Rei99], left figure).

Magnetic Field: We used a quadratic approximation of the B-field [Rei99]:

$$B = B_{max}\left(1 - \left(\frac{x}{l}\right)^2\right). \tag{4.1}$$

This approximation depends crucially on the magnetic field parameter l. Comparing this approximation with a magnetic field simulation of PERKEO II [Mae05], we find that $l = 740$ mm fits good in the region ± 50 mm around the maximum (figure 4.5). The field in this region defines the magnetic mirror effect. If we consider the edge effect, we have to take into account the field strength at the diaphragms placed about 107 mm next to the field maximum. A good fit in this region is obtained with $l = 690$ mm. Using this value for l does not change the field around the decay center. Hence we use $l = 690$ mm to generate the spectra.

4.2.2 The Magnetic Mirror Effect

The magnetic mirror effect described in chapter 3.2 does change the neutrino asymmetry B. Therefore we have to correct the measured spectra considering this effect. The shape of the magnetic field inside the decay volume is given by a quadratic approximation (4.1). Figure 4.6 shows the asymmetry B for electrons and protons measured in the same (B^1) and in opposite (B^2) hemispheres. The first two figures were generated by assuming the center of the neutron beam aligned with the maximum of the magnetic field. The corrections on B^1 and B^2 differ, since the reflection depends on the angle between the particle momenta and the magnetic field lines, figure 4.7. The relative angle of electron and proton emitted in the same hemisphere is large due to momentum conservation. This implies a large emission angle relative to the field lines, a high reflection probability and a bigger correction on B^1 compared to B^2.

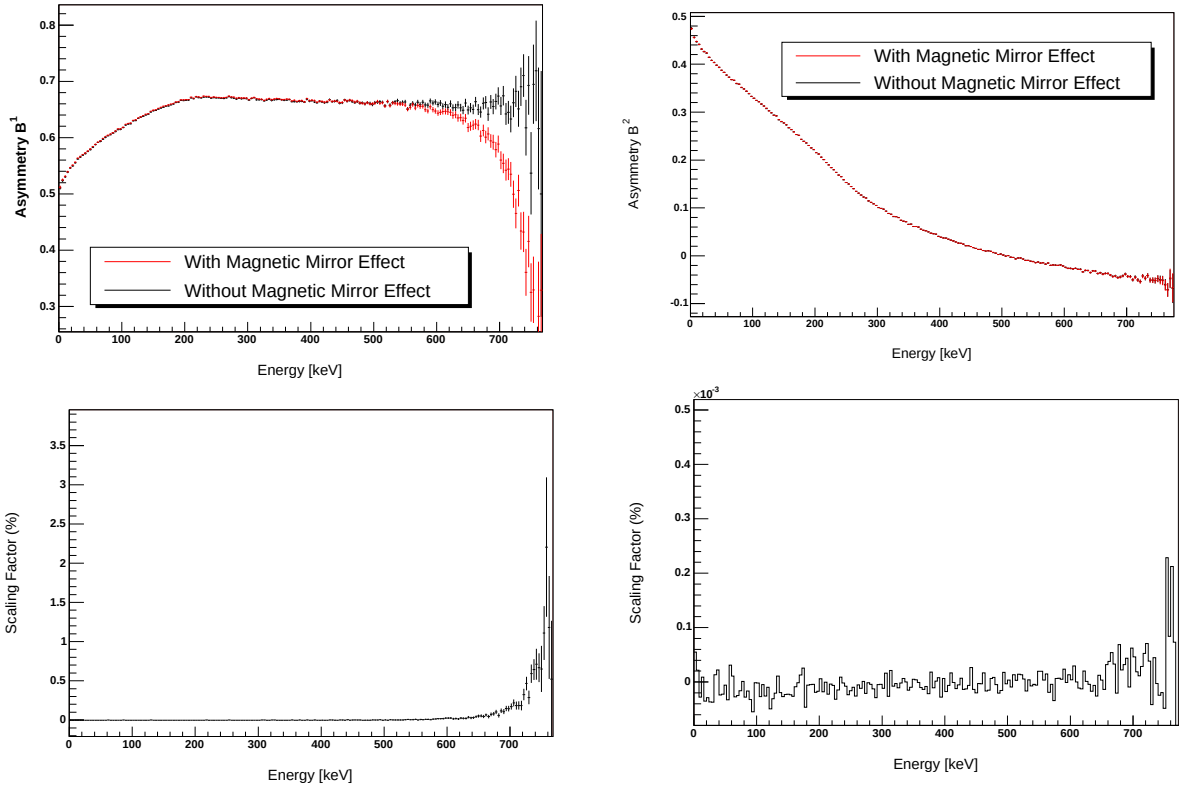

Figure 4.6: The magnetic mirror effect on the spectra of the asymmetry B: The upper histograms show the simulated spectra with and without mirror effect, the lower ones give the corrections on the measured spectra. B^1 is shown on the left, on the right B^2. The effect on B^2 is negligible since the scale of the ordinate is very small.

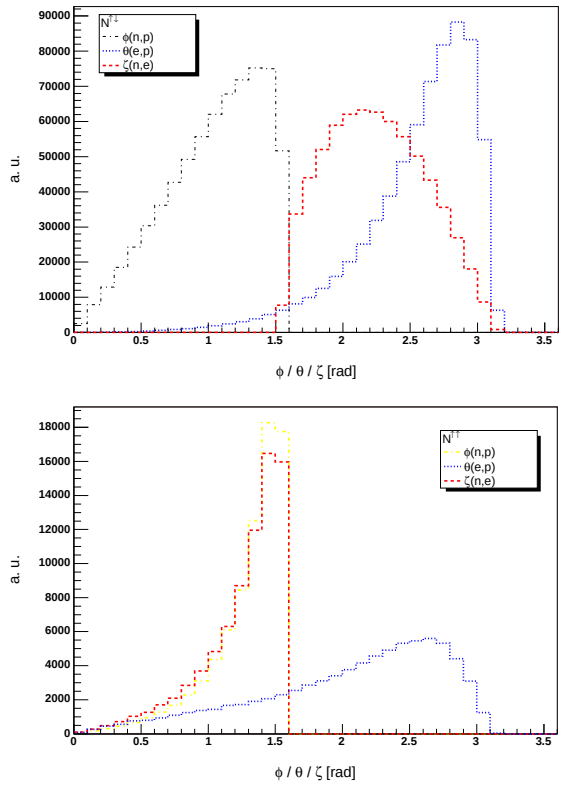

Figure 4.7: The two histograms show the angles between the direction of the neutron spin, electron momentum and proton momentum: $\Phi(n,p)$ denotes the angle between neutron spin and proton momentum, $\theta(e,p)$ is the angle between electron and proton, $\zeta(n,e)$ denotes the angle between neutron spin and electron. The upper figure gives the angles for electron and proton emitted in opposite hemispheres $N^{\uparrow\downarrow}$, the lower figure considers the emission of both particles in the same hemisphere $N^{\uparrow\uparrow}$.

4.2.3 The Electric Mirror Effect

The electric mirror effect describes the reflection of charged particles at electric potentials. In the experiment the potential of the carbon foils accelerates the protons towards the detectors, wheras the electrons are decelerated. Though the installed aluminium wires decrease the potential in the decay volume very effectively, there might be a small residual electric field. The shape of the electric potential has been simulated and can be described by a quadratic approximation in one dimension [Bra00]

$$V(x) = \frac{\delta E}{(\frac{d}{2})^2}(x-s)^2 + \delta E. \tag{4.2}$$

δE is the difference between the extremum of the potential and a point at a distance $\frac{b}{2}$ to it. The width of the decay volume along x is d and s denotes the displacement of the beam center in respect to the potential's extremum. The neutron decays at the point x. In the simulation we assumed a reach-through potential of $V(x) = 200$ mV (this assumption is very conservative since we expect a $V(x) < 100$ mV). Due to the opposite charges of electron and proton the effect is different for both particles:

- **Protons:** The electric mirror effect for protons can be described analog to the magnetic mirror effect. If the proton's emission direction points away from the decay

volume, they follow a decreasing potential (a negative parabola) and are accelerated. If they are emitted towards the decay center, the protons have to fly against a positive gradient and are reflected in case they have too less energy to get over the electric potential barrier.

- **Electrons:** Electrons follow a positive gradient regardless of their emission direction, since the carbon foils are set on negative potentials. An electron with an energy too low to pass the potential of the foils will be reflected from one foil to the other many times until it is absorbed by the aluminium wires. Reflected electrons are lost for the measurement.

We implemented the electric mirror effect for protons in the simulation and simulated spectra assuming a displacement $s = 0$. There was no change compared to spectra without this effect since the potential inside the decay volume is very small compared to the proton's energy. The number of reflected protons is therefore negligible.

The implementation of the electrons' electric mirror effect in the simulation was not possible so far. The difficulties arise since one has to consider the decreasing magnetic field together with the electric field. The momentum parallel to the magnetic field lines increases due to the negative gradient of the B-field, the momentum perpendicular to it decreases. Simultaneously the momentum parallel to the electric field, which is aligned with the B-field, decreases due to the electric field. Since we have to consider relativistic velocities for the electrons, we did not find a solution of the differential equation for this problem. An ansatz to simulate the motion iteratively, i.e. calculating the vectors of the momenta at one position and doing the same for many positions following each other at small intervalls, did not solve the problem with satisfactory accuracy.

We estimated the effect assuming an adiabatic change of the parallel momentum that is not affected by the negative electric potential. The electron can pass the potential if its kinetic energy $E_{kin||}$ (parallel to the electric field) after the momentum reorientation due to the magnetic field is equal or larger than the electric potential W. The following equation[1] gives the minimum energy $E_{kin,min}$ for electrons necessary to pass the potential barrier, in case they are emitted perpendicular to the magnetic field lines (worst case scenario):

$$E_{kin,min} = \sqrt{(W^2 + 2m_e W)(1 + \frac{B_2}{B_1 - B_2}) + m_e^2} - m_e \quad [\mathrm{ke}V], \quad c = 1. \tag{4.3}$$

$B_1 = 1.03$ T denotes the magnetic field strength in the center of the decay volume, $B_2 \approx 0.8$ T the field strength at the foil generating an energy barrier for electrons of $W = 20$ keV. $m_e = 511$ keV is the electron's mass in the rest frame. All electrons with an

[1] see apendix

$E_{kin,min} \approx 84$ keV pass the potential barrier and can be detected.

Fits on neutrino asymmetry B spectra will be made at higher energies ($E > 200$ keV), since in the energy region $E < 200$ keV the background is too high to obtain clean spectra. In addition it is favored to fit B^1 at higher energies since the spectrum becomes constant and is less sensitive to the detector function. Therefore we do not assume an effect on B due to the reflection of electrons at the electric potential.

4.2.4 Time of Flight Spectrum

During the experiment we measured the energy of electrons and protons emitted in β-decay, their angular distribution (we observed two hemispheres), and in addition the time-of-flight (Tof) spectrum of the protons. The latter spectrum gives the time protons need to reach the detector after being emitted in the decay volume. Since protons and electrons are emitted at the same time and electrons reach the detector almost instantly ($\sim$ 3 ns) after emission, their signal defines the start of the proton's time-of-flight measurement; it is stopped by the detection of the proton. The time-of-flight information helps to distinguish between proton events and background: After a certain time even the slowest protons reach the detector hence events measured after this time are due to background (see also chapter 3.1). Furthermore we are interested in the time-of-flight spectrum for a better understanding of the background.

We think that the high voltage background consists of high energetic particles (e.g. gamma rays, electrons, positrons) and also low energetic ions. Since we do not know origin and nature of the ions inside PERKEO II, we analysed the time-of-flight spectrum of the background proceeding as follows:

1. Simulation of the proton time-of-flight spectrum and comparison with the measured one in order to cross-check the quality of the simulation and to adjust simulation parameters.
2. Simulation of the background time-of-flight spectrum: By changing the mass and the starting position of background ions we try to generate the measured background spectrum.

4.2.4.1 ToF Spectrum of Protons

The path of protons towards the detectors can be divided into three characteristic sectors (see figure 4.8): Sector 1 defines the range from the decay volume to the beginning of the grounded wires. This sector is not influenced by an electric field (or the influence is negligible). The distance through the grid of aluminium wires defines sector 2. Here the

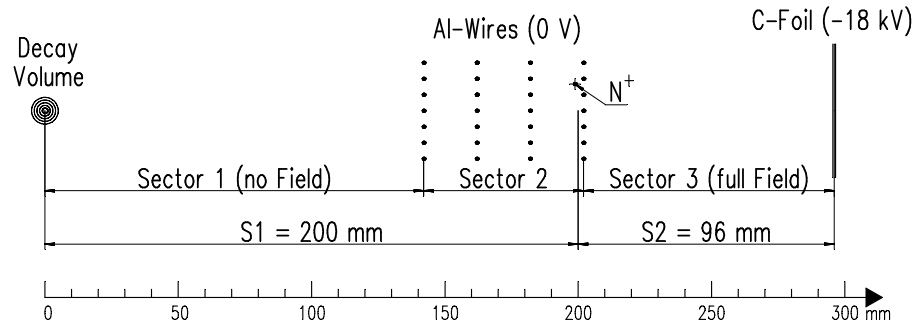

Figure 4.8: Simulation of the ToF-Spectra: The distance the protons have to cover from the decay volume to the carbon foil can be divided into three sectors. In the simulation these are reduced to two effective section S_1 and S_2. N^+ denotes a possible position at which N atoms may be ionised and cause background.

electric potential rises and the protons are accelerated. In sector 3, protons are accelerated onto the carbon foils with the complete force of the electric field. In the simulation we did not consider sector 2, and used just two sections: Section S_1 describes the motion in the magnetic field without an accelerating force, section S_2 considers both the B-field and the full electric field.

We used the time-of-flight spectra of protons (figures 4.9) to adjust the geometrical parameters S_1 and S_2 of the program. Data was taken with a potential of -18 kV. Coincident events detected in the same hemisphere emitted into the direction of the neutron spin are denoted with $N^{\uparrow\uparrow}$, events against the neutron spin $N^{\downarrow\downarrow}$. The simulation is in good agreement with the data, as can be seen in figure 4.10. The resulting parameters are $S_1 = 200$ mm and $S_2 = 96$ mm.

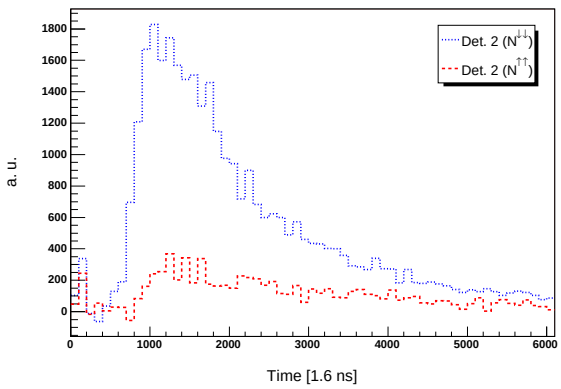

Figure 4.9: Proton ToF-spectrum for detector 2: The background data was subtracted from the time-of-flight data. The figure shows coincident events in the same hemisphere, electron and proton were emitted in ($N^{\uparrow\uparrow}$) or against ($N^{\downarrow\downarrow}$) the direction of the neutron spin. The big difference in count rate is due to the asymmetry B, which is close to unity.

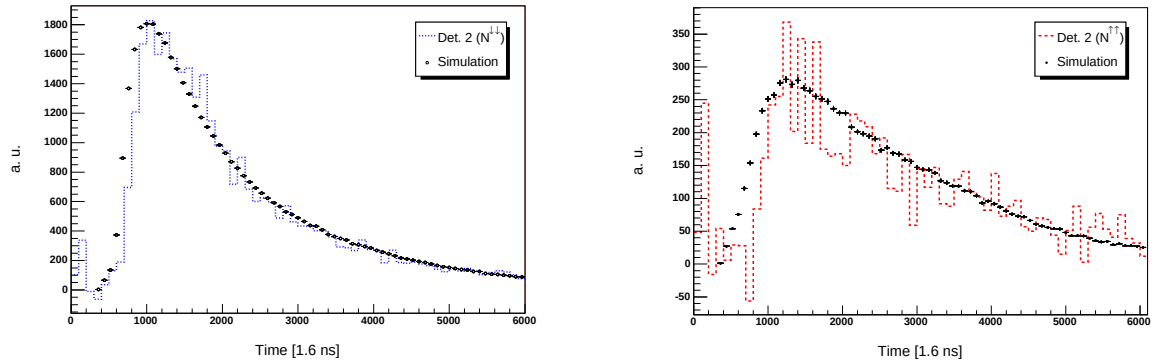

Figure 4.10: The simulated proton spectra plotted together with the measurement. Simulation and experiment agree very well.

4.2.4.2 ToF of the background

Figure 4.11 shows the time-of-flight specra of the background in the same hemisphere (measured without neutron beam). The usual background described by an exponential decay function seems to be superimposed by a Gaussian distribution. This peak could be caused by particles originating from inside the spectrometer, which may be produced at several positions:

- At the aluminium wires shielding the decay volume: High electric fields at the wires (diameter: 25 μm) could ionize atoms of the residual gas. Another effect may be caused by cosmic particles: They collide with the wires sputtering out aluminium ions.
- Between the grounding grids and the foil: cosmic rays entering the decay volume may hit remaining atoms and ionize them.
- At the carbon foils: other particles than protons passing the foil may produce many secondary electrons. These electrons are accelerated to the detector as well as towards

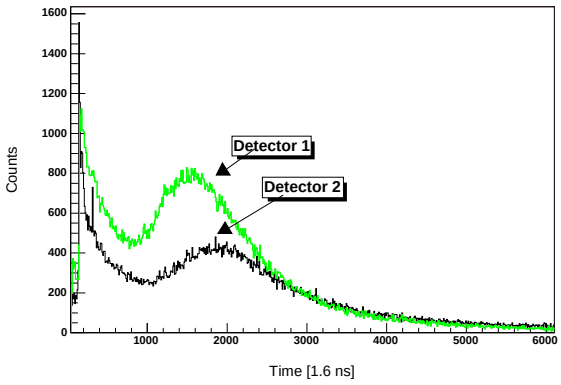

Figure 4.11: Background ToF-spectrum (with high voltage) for protons and electrons measured in the same hemisphere. A gaussian like peak superimposes the exponentially decaying background. The peak maximum of detector 1 occurs about 0.5 μs earlier than the one of detector 2.

the grounding grids. At the wires they may sputter aluminium ions or ionize atoms nearby.

In all cases the start and the stop signal may occur due to the formation of ion pairs.

We tried to reconstruct the peak by simulating several time-of-flight spectra: The pictures in figure 4.12 show the measured background of detector 2 together with the simulated peak. We considered the ions H^+, He^+, N^+ and Al^+, since hydrogen, helium and nitrogen are prominent constituents of the air. Aluminium was chosen since aluminium wires shielded the decay volume.

The initial kinetic energy of the particles was chosen to be very low ($E_{kin} \approx 25$ μeV), otherwise we could not fit the background peak properly. We defined a start range ΔX of the ions. This range begins at position X. If X_{foil} defines the x position of the foil, the maximum distance ions have to cover is $X_{foil} - X$, the minimum distance $X_{foil} - (X + \Delta X)$. The center of the decay volume is defined at $X = 0$, the section S_2 with the influence of the electric field begins 200 mm off the decay volume and is 96 mm long. The following geometrical parameters were determined to get the best agreement between simulation and data (see figure 4.12):

$$
\begin{array}{rrcll}
\mathbf{H^+}: & X & = & 193.5 & \text{mm} \\
 & \Delta X & = & 2 & \text{mm} \\
\mathbf{He^+}: & X & = & 196.7 & \text{mm} \\
 & \Delta X & = & 2 & \text{mm} \\
\mathbf{N^+}: & X & = & 198.3 & \text{mm} \\
 & \Delta X & = & 1.1 & \text{mm} \\
\mathbf{Al^+}: & X & = & 198.9 & \text{mm} \\
 & \Delta X & = & 0.7 & \text{mm}
\end{array}
$$

The He^+ and N^+ ions show the best agreement with the data, whereas the peak of the lighter H^+ is too narrow and does not fit to the background. The histogram for Al^+ - that also describes the data not satisfactory - demonstrates the heavier the atoms the sharper is the decline of the number of slow ions.

The value X of the He^+ and the N^+ spectra gives evidence that these particles could be emitted from a region within the aluminium wires. It is very likely that these ions produce the backgorund, since nitrogen is the most prominent constituent of air and since it is very difficult to remove helium out of the vacuum system. Hence both ions are present in the resudial gas.

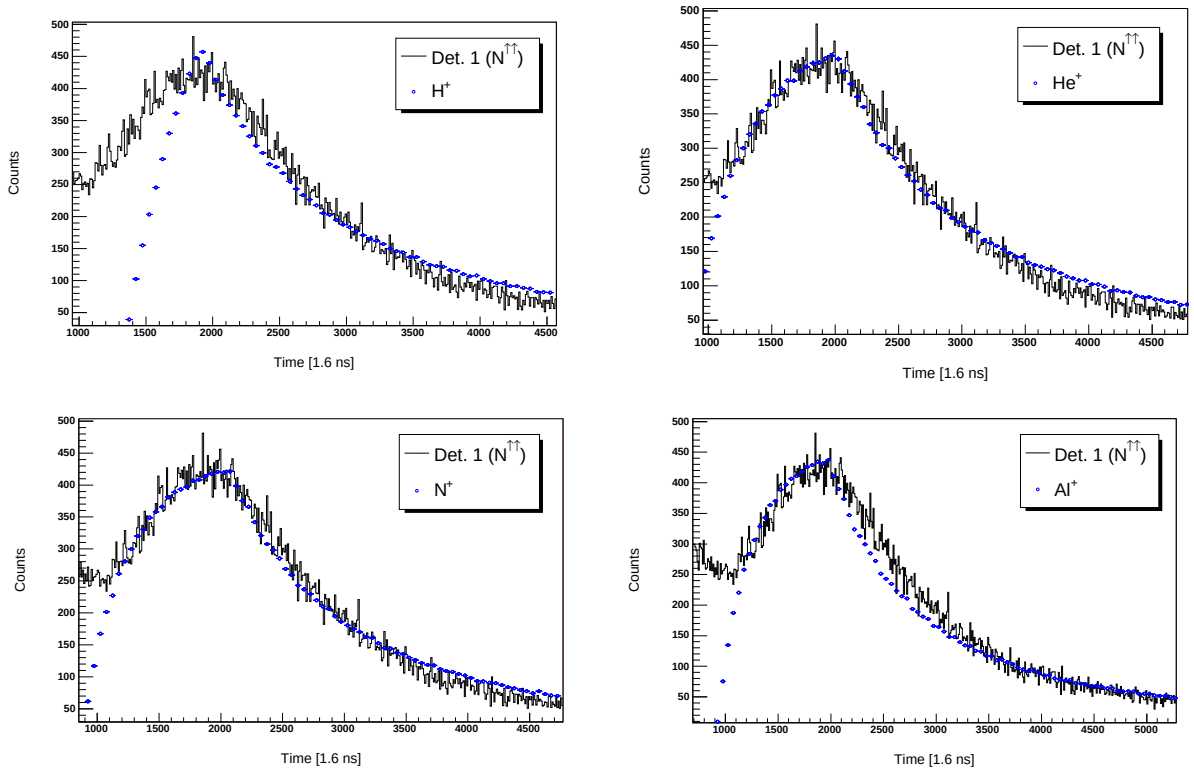

Figure 4.12: The peak in the high-voltage background of detector 2 (not of detector 1 as printed in the legend) superimposed by simulated time-of-flight spectra for H^+, He^+, N^+, and Al^+. He^+ and N^+ give results consistent with the data.

The shift of background peaks: The background peak measured with detector 1 differs from the peak obtained with detector 2 (figure 4.11): More background is measured in detector 1 and the peak appears $\sim$ 0.5 μs. This shift may be caused by a known asymmetry in our setup: The distance between detector and foil was $\sim$ 180 mm for detector 1 and $\sim$ 200 mm for detector 2.

Considering this geometrical displacement, the difference in the time-of-flight spectra could be caused by

1. electrons emitted from the foil due to an impact of charged particles (except protons)
2. ions moving from the foil to the detector.

Electrons cannot be the reason for the time shift of the peaks since their velocity is much to high: They pass 20 mm in just $\Delta t \approx 0.3$ ns. Ions could cause the time displacement in two ways: Either an ion is emitted from the scintillator to the foil (and produces secondary electrons there that are detected) or an ion becomes neutral while flying through the foil and hits the detector as a neutral particle.

We made the following simple estimations from which we can exclude two scenarios:

- **Ions emitted from the scintillator:** The velocitiy of ions to cover 20 mm in 0.5 μs is $v_{ion} \approx 40000$ m s^{-1}. We estimate the mass of an ion m_{ion} which is accelerated to v_{ion} by the electric field (-18 kV). This mass is very large so that we exclude this possibility: We do not expect that very big molecules occur in the spectrometer.
- **Ions passing the foil:** We assume that an ion can fly through the foil. While passing it, the ion can collect an electron and move towards the detector. In this case the velocity of the neutral particle has to be $v_{neutral} \approx 40000$ m s^{-1}. From the ToF-simulation we obtain the mean velocity of a He^+-ion to be $v_{He^+} \approx 10^5$ m s^{-1}, hence $v_{He^+} > v_{neutral}$. Thus an ion must loose much energy in the foil. This possibility is excluded since the foil is very thin.

The most promising possibility that could lead to the difference in the time of flight spectra does not consider the distances between foils and detectors: If the atoms are ionized at slightly different positions (e.g. due to inhomogenities in the wires or smaller shielding of the electric field), even a very small spatial difference (below 1 mm) would yield the measured situation: On the side of detector 1, N or He atoms are ionized closer to the detector compared to side 2.

The simulation of the backgound ToF-spectrum of detector 1 supports this hypothesis: The peak is fitted very well by N^+ ions generated at a position slightly closer to the foil (figure 4.13).

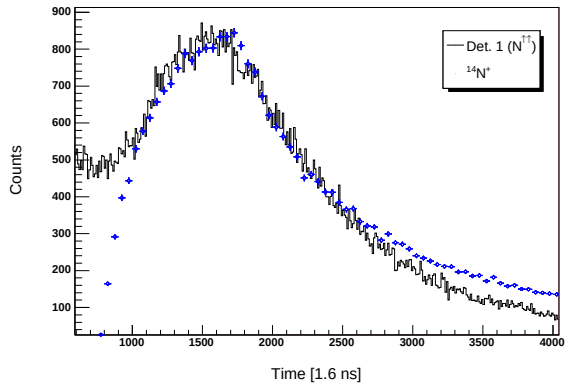

Figure 4.13: Measurement and simulation of the high-voltage background of detector 1: It is again consistent with a N^+ ToF-spectrum.

Chapter 5

PERKEO III

The experiment to determine the neutrino asymmetry B described in this thesis was performed with the spectrometer PERKEO II: Two superconducting coils produce a magnetic field perpendicular to the neutron beam. The β-decay products are guided along the field lines towards the detectors, and we obtain a full $2 \times 2\pi$ detector. Due to the setup, we are limited in statistics (the maximal length of the decay volume is approximately 30 cm) and have to deal with several systematic effects, like the magnetic mirror effect and the edge effect. The most critical systematic effect - limiting the results with PERKEO II - is the beam related background that can not be removed from the spectra.

Hence, a new instrument PERKEO III is designed to examine neutron β-decay with better systematics and highest accuracy. Using a chopped neutron beam, the beam related background will be reduced to zero. PERKEO III still features the "PERKEO principle": A magnetic field divides the spectrometer into two 2π hemispheres.

5.1 The Instrument PERKEO III

A sketch of the spectrometer PERKEO III is shown in figure 5.1. The magnetic field of this instrument is parallel to the neutron beam, hence the neutron spin has to point in or against flight direction. A chopper installed in front of the spectrometer produces bunches of cold neutrons. Compared to PERKEO II, this setup has the following advantages [Mae05]:

- A non-subtractable beam related background is avoided: Data will be taken only if the chopper is closed (no background from the beamline) and no neutrons hit the beam stop. In addition monitoring of time dependent background is possible since signal and background are measured under the same conditions (due to short chopper intervalls).
- The magnetic mirror effect is negligible: Data is taken only while the neutron cloud is within the homogeneous part of the magnetic field.

- There is no edge effect: The whole neutron cloud is projected onto the detectors.

The instrument is designed to reach an ultra high vacuum ($\sim 10^{-9}$ mbar). In this way we decrease the probability that neutrons, electrons, and protons are scattered on atoms of the residual gas and are lost for the measurement. Additionally, the background due to ions produced in collisions will be negligible.

Detector Design of PERKEO III: The detector design of PERKEO III is the same as used with PERKEO II: Neutron decay particles depose energy in a scintillator, the energy will be converted into photons that are guided by lightguides to photomultiplier tubes. We will again use two detectors to cover both hemispheres.

Compared to the detectors used in former PERKEO II experiments, the dimensions of the new detector will be much bigger: about 300×400 mm^2. This size is neccessary since the new spectrometer will have a decay volume length of about 2 m to obtain a homogeneous magnetic field in the center of the decay volume. The diameter of the vacuum vessel has

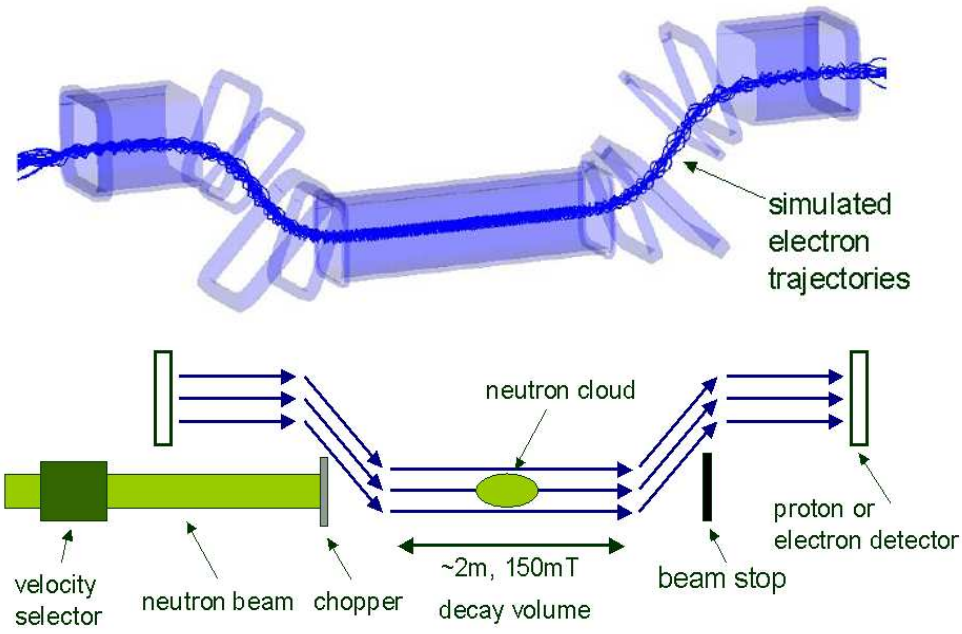

Figure 5.1: The new instrument PERKEO III: Upper figure: Simulation of electron trajectories with the realized coil configuration [Mae05]. Lower figure: Schematic drawing of the experimental setup. The magnetic field is aligned parallel to the neutron beam axis. Using a neutron chopper installed in front of the spectrometer, bunches of neutrons are produced which allow to do a background free measurement.

to be ~ 0.5 m because the cross section of the beam diverges from about 50 mm at the beginning of the spectrometer to about 150 mm at the end of the decay volume. In addition we have to consider the maximum gyration radius $r_{gyr} \approx 30$ mm of electrons and protons in the magnetic field $B \approx 150$ mT, which makes a large vacuum chamber diameter necessary.

Due to the dimensions of the new detector, it is not possible to attach the photomultiplier tubes directly to the back of the detector as done in the B-measurements: The effective area of one photomultiplier tube is about 1000 mm^2, so only a large amount of photomultiplier tubes would accomplish a read out without big losses. Therefore, we will extract the light from the detector sides.

We have a scintillator thickness of 5 mm, its height will be approximately 380 mm: To cover an area of about 1900 mm^2, we will need three photomultiplier tubes. Since the readout will be done from both sides of each detector, twelve photomultiplier tubes will have to used altogether. Since the same number of photomultiplier tubes was installed in the PERKEO IIB experiment, we know that the expected data can be processed by the existing data acquisition system.

Such big detectors must be prevented against stress since this can cause capillary cracks in the lightguide. These cracks decrease the efficiency of the lightguide and information is lost. A stiff aluminium frame, on which we attach the scintillators and the lightguides together with the photomultiplier tubes, will provide the necessary stability (figure 5.2). The aluminium frame is pushed into the vacuum chamber from the side: Little rails ensure an easy movement into the chamber, define the exact position of the system inside the vacuum and give the necessary stabilisation of the frame.

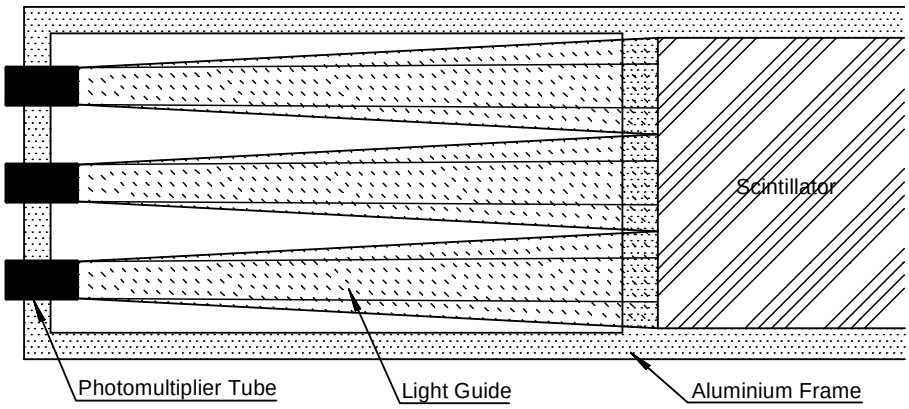

Figure 5.2: PERKEO III detector: The lightguides are attached on a stiff aluminium frame together with the photomultiplier tubes. This prevents the sensitive scintillator and lightguide materials against stress and conserves the required qualitiy of the detection system for a long measurement period. Only a part of the scintillator is drawn in the figure.

5.2 Physical Motivation for PERKEO III

Within the Standard Model, the CKM matrix (2.11) describes quark mixing in weak interactions. If the matrix is unitary, the first row yields

$$V_{ud}^2 + V_{us}^2 + V_{ub}^2 = 1. \tag{5.1}$$

V_{ud} is obtained in neutron decay by measuring the electron asymmetry A

$$A = \frac{N^{\downarrow} - N^{\uparrow}}{N^{\downarrow} + N^{\uparrow}}, \tag{5.2}$$

and the neutron liftetime τ. $N^{\downarrow}$ denotes the number of electrons emitted opposite to the neutron spin, whereas the momentum of $N^{\uparrow}$ points parallel to the neutron spin. Former experiments which determined the matrix elements gave hints on a possible non-unitarity of the CKM-matrix, i.e. a deviation from the Standard Model [Abe02], [Har03], [Abe04], figure 5.3.

A task for future experiments - including PERKEO III - is the revisal of these deviations: More precise measurements may confirm or reject the actual values. But also the determination of small parameters like the weak magnetism A^{wm} and the fierz term is a challenge: A^{wm} is energy dependent and changes the asymmetry A slightly at high energies[1], the fierz term changes the β-spectrum at low energies. These small effects may be observed when good statistics and a well configured detection system are obtained.

[1]The weak magnetism can also be extraced from a measurement of the difference spectrum $N^{\downarrow} - N^{\uparrow}$: This spectrum is background free, but here we need a very good detector function in order to extract A^{wm}.

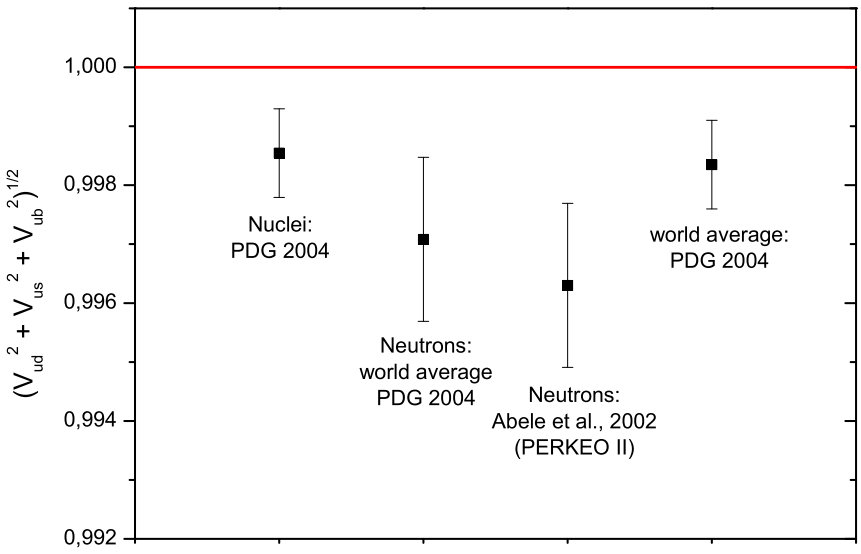

Figure 5.3: Unitarity of the first row of the CKM matrix: Results obtained with V_{ud} measured by different groups in neutron decay and superallowed β-decays give a deviation from unitarity.

Chapter 6

Summary

In summer 2004, we did a measurement of the neutrino asymmetry B in neutron β-decay with PERKEO II. The experiment took place at the cold neutron beam place PF1b of the ILL, France. The coefficient B describes the correlation between neutron spin and neutrino momentum. A precise determination of B may verify the Standard Model, and can give constraints on theories beyond the Standard Model. Therefore, we considerably improved the setup compared to the asymmetry B measurement in 2001 [Kre05a]:

- Using two supermirror polarizers changed the degree of polarization P from 98.7(5) % [Kre04] between 3.2 and 13.0 Å to 99.7(1) % [Schu04] between 2 and 12 Å.
- A new data acquisition system allowed to reduce systematic effects that limited the 2001 measurement.
- More vacuum pumps produced an average vacuum of about $1 \cdot 10^{-6}$ mbar. The experiment was done with the best vacuum ever reached with the spectrometer PERKEO II.
- The high voltage setup was planned with much effort to avoid sharp edges that can cause high fields leading to disturbing effects.
- An improved beamstop reduced the beam related background.

The improvements should allow to determine the asymmetry B with higher precision: We had more measuring time than the 2001 experiment, and detector 2 was configured very well. Though we measured much high voltage background at detector 1 we expect to have more statistics than the former experiment.

We aligned the center of the neutron beam with the magnetic field to reduce the change of the asymmetry B due to the magnetic mirror effect. Furthermore, we decreased

the cross section of the beam with an additional diaphragm to minimize the effect. The copper foil activation analysis was used to determine the position and the shape of the neutron beam. The measurements showed no displacement D_x between the beam and the magnetic field, $D_x = (1.1 \pm 1.4)$ mm.

The used detector area was quite large: We used a scanner to determine the detector function, which should be as homogeneous as possible [Bre03]. The scanner moves a calibration source at defined positions in front of the detector. We developped an improved control software, which allowed the scanner to reach given positions with high accuracy and as fast as possible. Multiple calibration positions can be reached automatically.

The measured spectra have to be corrected due to systematic effects, like the magnetic and electric mirror effect, and the edge effect. We wrote a Monte Carlo Simulation of the neutron β-decay within the environment of PERKEO II. We simulated asymmetry B spectra without and with systematic effects. Comparing these spectra, we obtain the correction on the measured spectrum: The asymmetry B^1 has to be corrected less than 0.04 % for electron energies $E_e < 600$ keV due to the magnetic mirror effect, the asymmetry B^2 is not affected. The electric mirror effect is negligible.
Furthermore, we simulated the time-of-flight spectrum of ions inside the spectrometer to examine the origin of measured background: The background is generated in the region of the grounded aluminium wires and probably due to He^+ and N^+ ions.

The CKM element V_{ud} can be obtained from the electron asymmetry A and the neutron's lifetime τ. Former measurements show that the first row of the matrix deviates from unitarity. These results may be verified or rejected by new experiments, like our new spectrometer PERKEO III: This spectrometer will determine the correlation coefficients in neutron β-decay with even higher accuracy. The use of a chopper will set the beam related background to zero, edge effects will not occur since the whole neutron bunch is projected onto the detector, and the magnetic mirror effect will be negligible. Furthermore, this instrument may allow to determine small terms occuring in neutron decay, like the fierz term and the weak magnetism A^{wm}, which never before have been determined in neutron decay. First studies of possible experiments with PERKEO III have been made.

Appendix A

Pseudo Code to control the Calibration Scanner

In chapter 3.3.2, the basic ideas behind the control software of the Calibration Scanner were explained. Here we give a pseudo code of the algorithm to present the program logic in some more detail:

The used fonts denote:

Function	: (call of) a function,
`position`	: common variable,
`WHILE`	: command,
`Output`	: comment about the program action,
STEPCOND	: defined values; STEPCOND defines the distance to cover reasonably in step-mode, JUMP_ALLOWANCE is the allowed deviation from the target position.

Main Function:

```
target = GetTargetPosition
position = GetPosition
move = 1
noftry = 0
jumpcalls = 0

WHILE ((move != 0) AND (noftry < MAX_NO_OF_TRY))
{
      IF (move < 0 ) IncreaseControlVoltage
      noftry = noftry+1
      togo = |target-postion|
      IF (noftry = MAX_NO_OF_TRY) GoToNextTarget

              IF ((togo <= STEPCOND) OR (jumpcalls >= MAX_NO_OF_JUMPCALLS))
              {
                  move = return of Step Function
              }
              ELSE
              {
                  return = return of Jump Function
                  IF (return = JUMP_OUT_OF_RANGE
                  {
                      move = 0 AND Output:  'Undefined Range'
                  }
                  IF (return = VOLTAGE_TOO_LOW)
                  {
                      move = -1 AND jumpcalls+1
                  }
                  IF (return = TOO_MANY_JUMPS)
                  {
                      move = 1 AND jumpcalls = MAX_NO_OF_JUMPCALLS
                  }
                  IF (return = JUMP_OK)
                  {
                      move = 1
                  {
      }
}
position = GetPosition
END
```

Jump Function

```
jumpnumber = 0
nof_too_short_jumps = 0

WHILE ((|(target - newposition)| > JUMP_ALLOWANCE)
              AND (jumpnumber < MAX_NOF_JUMPS))
{
    jumpnumber = jumpnumber+1
    lastposition = GetPosition
    ApplyVoltage
    Wait
    SetVoltage=0
    newposition = GetPosition

    IF ((newposition-lastposition) < MIN_WAY)
    {
      nof_too_short_jumps = nof_too_short_jumps + 1
    }
    ELSE
    {
      nof_too_short_jumps = 0
    }
    IF (nof_too_short_jumps > NOF_TOO_SHORT_JUMPS)
    {
      return = VOLTAGE_TOO_LOW
    }
}
IF (jumpnumber >= MAX_NOF_JUMPS)
{
    return = TOO_MANY_JUMPS
}
return = JUMP_OK
```

Step Function

```
stepnumber = 0
nof_too_short_steps = 0

WHILE ((|(newposition - target)| < STEP_ALLOWANCE)
              AND (jumpnumber < MAX_NOF_STEPS))
{
    stepnumber = stepnumber+1
    lastposition = GetPosition
    ApplyVoltage
    Wait
    SetVoltage=0
    newposition = GetPosition

    IF((newposition-lastposition) < MIN_WAY)
    {
      nof_too_short_steps = nof_too_short_steps + 1
    }
    ELSE
    {
      nof_too_short_steps = 0
    }
    IF( nof_too_short_steps > NOF_TOO_SHORT_STEPS)
    {
      return = -1
    }
}
IF(stepnumber >= MAX_NOF_STEPS)
{
      return = -1
}

return = 0
```

Appendix B

Estimation of the electric mirror effect

In chapter 4.2.3 we introduced the electric mirror effect and estimated its influence on the electron spectrum. Below, we give the derivation of this estimation:

We first have to consider the change of the angle θ between the momentum of the electron and the magnetic field lines due to the decreasing magnetic field. This angle can be obtained by considering the magnetic mirror effect:

$$\sin\theta_{crit} = \sqrt{\frac{B_1}{B_{max}}}. \tag{B.1}$$

B_1 is the magnetic field strength at the emission point of the particle, B_{max} is the maximum field strength. In case $\theta \geq \theta_{crit}$, the particle is reflected by the magnetic field (we do not consider this case here).

Assuming the condition (B.1), a particle is emitted at point 1 with θ_1. The angle between mometum and magnetic field for the same particle at point 2 is θ_2, obtained by (B.1) substituting B_1 by B_2. This way we obtain an equation between θ_1 and θ_2:

$$\sin\theta_1 = \sin\theta_2 \sqrt{\frac{B_1}{B_2}} \tag{B.2}$$

We will come back to (B.2) later and go on with the relation of the energies. The kinetic energy of the electron has to be $E_{kin} \leq e \cdot U$ to get over the potential barrier. e denotes the electron charge, U the applied voltage. Considering relativistic velocities, we get

$$\begin{aligned} e \cdot U &= m_0 c^2 (\gamma - 1) \\ &= \sqrt{\mathbf{p}'^2 c^2 + m_0^2 c^4} - m_0 c^2 \end{aligned} \tag{B.3}$$

and solve for $\mathbf{p'}^2c^2$:

$$\mathbf{p'}^2c^2 = (eU)^2 + 2m_0c^4eU. \tag{B.4}$$

Since only the momentum parallel to the magnetic field is changed, the obtained

$$\mathbf{p'} = \mathbf{p}\cos\theta_2, \tag{B.5}$$

for $\mathbf{p}$ is the momentum of the particle and its energy

$$E^2 = (\mathbf{p}^2\cos^2\theta_2 + \mathbf{p}^2\sin^2\theta_2)c^2 + m_0^2c^4. \tag{B.6}$$

We can write this

$$E^2 = (\mathbf{p}^2\cos^2\theta_2 \left(1 + \frac{\sin^2\theta_2}{\cos^2\theta_2}\right))c^2 + m_0^2c^4 \tag{B.7}$$

and with (B.2)

$$E^2 = (\mathbf{p}^2\cos^2\theta_2 \left(1 + \frac{\sin^2\theta_1 \cdot B_2}{\cos^2\theta_2 \cdot B_1}\right))c^2 + m_0^2c^4. \tag{B.8}$$

Now we insert (B.4) and substitute θ_2 by θ_1

$$E^2 = ((eU)^2 + 2m_0c^4eU \left(1 + \frac{\sin^2\theta_1 \cdot B_2}{1 - \sin^2\theta_1 \cdot B_2/B_1}\right))c^2 + m_0^2c^4 \tag{B.9}$$

Assuming the worst case scenario, i.e. the electron is emitted perpendicular to the magnetic field lines, we set $sin\theta_1 = 1$ and obtain the given equation

$$E_{kin,min} = \sqrt{(W^2 + 2m_eW)(1 + \frac{B_2}{B_1 - B_2}) + m_e^2} - m_e \quad [\mathrm{k}eV], \tag{B.10}$$

with $W = eU$ and $c = 1$.

Bibliography

[Abe00] H. Abele, Nucl. Instr. Meth. A **440** (2000) 499-510

[Abe02] H. Abele, M. Astruc Hoffmann, S. Baeßler, D. Dubbers, F. Glück, U. Müller, v. Nesvizhevsky, J. Reich, O. Zimmer, *Is the Unitarity of the Quark-Mixing CKM Matrix Violated in Neutron β-Decay?*, Phys. Rev. Lett. **88** 211801 (2002)

[Abe04] H. Abele, E. Barberio, D. Dubbers, F. Glück, J. C. Hardy, W. J. Marciano, A. Serebrov, N. Severijns, *Quark mixing, CKM unitarity*, Eur. Phys. J. C 33, 1-8 (2004)

[Ait89] I. J. R. Aitchison, A. J. Hey: *Gauge Theories in Particle Physics*, Adam Hilger, Bristol 1989

[Bae96] S. Baeßler, Ph.D. thesis, University of Heidelberg 1996

[Bra00] B. Brand, Diploma thesis, University of Heidelberg 2000

[Bre03] M. Brehm, Diploma thesis, University of Heidelberg 2003

[Har03] J. C. Hardy, I. S. Towner: *Superallowed* $0^+ \rightarrow 0^+$ *Beta Decay: Current Status and Future Prospects*, in H. Abele and D. Mund (eds.) *Quark-Mixing, CKM-Unitarity*, Mattes Verlag, Heidelberg (2003)

[Jac57] J. D. Jackson et al., Phys. Rev. **106**, 517 (1957)

[Jac02] J. D. Jackson: *Klassische Elektrodynamik*, de Gruyter, Berlin 2002

[Kre04] M. B. Kreuz, Ph.D. thesis, University of Heidelberg 2004

[Kre05a] M. B. Kreuz et al.: *A Measurement of the Antineutrino Asymmetry B in Free Neutron Decay*, submitted to Phys. Lett. B

[Kre05b] M. B. Kreuz et al., accepted from Nucl. Instr. Meth. A (2005)

[Krem04] J. Krempel, Diploma thesis, University of Heidelberg 2004

[Lee56] T. D. Lee, C. N. Yang: *Question of Parity Conservation in Weak Interactions*, Phys. Rev. **104**(1), 254 (1956)

[Leo94] W. R. Leo: *Techniques for Nuclear and Particle Physics Experiments*, Springer, Heidelberg 1994

[Mae05] B. Märkisch, private communication

[Moh75] R. N. Mohapatra et al., Phys. Rev. Lett. **68**, 3499 (1992)

[Mun05] D. Mund, private communication

[PDG04] S.Eidelman et al., Phys. Lett. B **592**, 1 (2004)

[Plo00] C. Plonka, diploma thesis, University of Heidelberg 2000

[Pov01] B. Povh et al.: *Teilchen und Kerne*, Springer, Heidelberg 2001

[Schu04] M. Schumann, Diploma thesis, University of Heidelberg 2004

[Schu05] M. Schumann, private communication

[Rei99] J. Reich, Ph.D. thesis, University of Heidelberg 1999

[Rein91] R. Reiner, Diploma thesis, University of Heidelberg 1991

[Wil82] D. H. Wilkinson, Nucl. Phys. **A337**, 474 (1982)

[Wu57] C. S. Wu et al., Physical Review **105**, 1413 (1957)

[Yer00] B. G. Yerozolimsky, Nucl. Instr. Meth. A **440** (2000), 491-498

Erklärung:

Ich versichere, daß ich diese Arbeit selbständig verfasst und keine anderen als die angegebenen Quellen und Hilfsmittel benutzt habe.

Heidelberg, den 17. Mai 2005